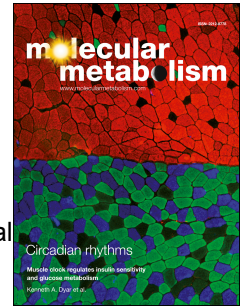


Journal Pre-proof

Peptide-YY₃₋₃₆/Glucagon-Like Peptide-1 Combination Treatment of Obese-Diabetic Mice Improves Insulin Sensitivity associated with Recovered Pancreatic β -Cell Function and Synergistic Activation of Discrete Hypothalamic and Brainstem Neuronal Circuitries



Brandon B. Boland, Rhianna C. Laker, Siobhan O'Brien, Sadichha Sitaula, Isabelle Sermadiras, Jens Christian Nielsen, Pernille Barkholt, Urmaz Roostalu, Jacob Hecksher-Sørensen, Sara Rubek Sejthen, Ditte Dencker Thorbek, Arthur Suckow, Nicole Burmeister, Stephanie Oldham, Sarah Will, Victor G. Howard, Benji M. Gill, Philip Newton, Jacqueline Naylor, David C. Hornigold, Jotham Austin, Louise Lantier, Owen P. McGuinness, James L. Trevaskis, Joseph S. Grimsby, Christopher J. Rhodes

PII: S2212-8778(21)00247-7

DOI: <https://doi.org/10.1016/j.molmet.2021.101392>

Reference: MOLMET 101392

To appear in: *Molecular Metabolism*

Received Date: 22 July 2021

Revised Date: 22 October 2021

Accepted Date: 4 November 2021

Please cite this article as: Boland BB, Laker RC, O'Brien S, Sitaula S, Sermadiras I, Nielsen JC, Barkholt P, Roostalu U, Hecksher-Sørensen J, Sejthen SR, Thorbek DD, Suckow A, Burmeister N, Oldham S, Will S, Howard VG, Gill BM, Newton P, Naylor J, Hornigold DC, Austin J, Lantier L, McGuinness OP, Trevaskis JL, Grimsby JS, Rhodes CJ, Peptide-YY₃₋₃₆/Glucagon-Like Peptide-1 Combination Treatment of Obese-Diabetic Mice Improves Insulin Sensitivity associated with Recovered Pancreatic β -Cell Function and Synergistic Activation of Discrete Hypothalamic and Brainstem Neuronal Circuitries, *Molecular Metabolism*, <https://doi.org/10.1016/j.molmet.2021.101392>.

This is a PDF file of an article that has undergone enhancements after acceptance, such as the addition of a cover page and metadata, and formatting for readability, but it is not yet the definitive version of record. This version will undergo additional copyediting, typesetting and review before it is published

in its final form, but we are providing this version to give early visibility of the article. Please note that, during the production process, errors may be discovered which could affect the content, and all legal disclaimers that apply to the journal pertain.

© 2021 Published by Elsevier GmbH.

1 **Peptide-YY₃₋₃₆/Glucagon-Like Peptide-1 Combination Treatment of Obese-Diabetic Mice Improves**
2 **Insulin Sensitivity associated with Recovered Pancreatic β -Cell Function and Synergistic Activation of**
3 **Discrete Hypothalamic and Brainstem Neuronal Circuitries**

4 Brandon B. Boland^{1,2,4}, Rhianna C. Laker¹, Siobhan O'Brien³, Sadichha Sitaula¹, Isabelle Sermadiras³, Jens
5 Christian Nielsen², Pernille Barkholt², Urmaz Roostalu², Jacob Hecksher-Sørensen², Sara Rubek Sejthen²,
6 Ditte Dencker Thorbek², Arthur Suckow^{1,5}, Nicole Burmeister^{3,6}, Stephanie Oldham¹, Sarah Will¹, Victor
7 G. Howard¹, Benji M. Gill¹, Philip Newton³, Jacqueline Naylor¹, David C. Hornigold¹, Jotham Austin⁷,
8 Louise Lantier⁸, Owen P. McGuinness⁸, James L. Trevaskis^{1,9}, Joseph S. Grimsby¹, Christopher J. Rhodes^{1†}

9 ¹*Research and Early Development, Cardiovascular, Renal and Metabolism, BioPharmaceuticals R&D,*
10 *AstraZeneca, Gaithersburg, MD, USA, and Cambridge, UK*

11 ²*Gubra ApS, Hørsholm, Denmark*

12 ³*Antibody and Protein Engineering, BioPharmaceuticals R&D, AstraZeneca., Gaithersburg, MD, USA, and*
13 *Cambridge, UK*

14 ⁴*Current address: PRECISIONscientia, Yardley, PA, USA*

15 ⁵*Current address: DTX Pharma, San Diego, CA, USA*

16 ⁶*Current address: Roche, Penzberg, Germany*

17 ⁷*University of Chicago Advanced Electron Microscopy Core Facility, Chicago, IL, USA*

18 ⁸*Vanderbilt University Mouse Metabolic Phenotyping Center, Nashville, TN, USA*

19 ⁹*Current address: Gilead Sciences, Foster City, CA, USA*

20 **Keywords:** Diabetes; obesity; insulin sensitivity; pancreatic β -cell; hypothalamus

21 **†Corresponding author:**

22 Christopher J. Rhodes Ph.D.
23 Cardiovascular, Renal and Metabolism, Biopharmaceuticals R&D
24 AstraZeneca
25 One Medimmune Way
26 Gaithersburg, MD 20878, USA
27 T: 301-398-4791 C: 301-204-3673
28 christopher.rhodes@astrazeneca.com
29

1 Abstract

2 Objective: Obesity-linked type 2 diabetes (T2D) is a worldwide health concern and many novel
3 approaches are being considered for its treatment and subsequent prevention of serious comorbidities.
4 Co-administration of glucagon like peptide 1 (Fc-GLP-1) and peptide YY₃₋₃₆ (Fc-PYY₃₋₃₆) renders a
5 synergistic decrease in energy intake in obese men. However, mechanistic details of the synergy
6 between these peptide agonists and their effects on metabolic homeostasis remain relatively scarce.

7 Methods: In this study, we utilized long-acting analogues of GLP-1 and PYY₃₋₃₆ (via Fc-peptide
8 conjugation) to better characterize the synergistic pharmacological benefits of their co-administration
9 on body weight and glycaemic regulation in obese and diabetic mouse models. Hyperinsulinemic-
10 euglycemic clamps were used to measure weight-independent effects of Fc-PYY₃₋₃₆ + Fc-GLP-1 on insulin
11 action. Fluorescent light sheet microscopy analysis of whole brain was performed to assess activation of
12 brain regions.

13 Results: Co-administration of long-acting Fc-IgG/peptide conjugates of Fc-GLP-1 and Fc-PYY₃₋₃₆ (specific
14 for PYY receptor-2 (Y2R)) resulted in profound weight loss, restored glucose homeostasis, and recovered
15 endogenous β -cell function in two mouse models of obese T2D. Hyperinsulinemic-euglycemic clamps in
16 C57BLKS/J *db/db* and diet-induced obese Y2R-deficient (Y2RKO) mice indicated Y2R is required for a
17 weight-independent improvement in peripheral insulin sensitivity and enhanced hepatic glycogenesis.
18 Brain cFos staining demonstrated distinct temporal activation of regions of the hypothalamus and
19 hindbrain following Fc-PYY₃₋₃₆ + Fc-GLP-1R agonist administration.

20 Conclusions: These results reveal a therapeutic approach for obesity/T2D that improved insulin
21 sensitivity and restored endogenous β -cell function. This data also highlights the potential association
22 between the gut-brain axis in control of metabolic homeostasis.

23 Keywords

24 Glucagon-like peptide-1 (GLP-1), Peptide-YY₃₋₃₆ (PYY₃₋₃₆), β -cell function, diabetes remission, insulin
25 sensitivity, central nervous system, glucose homeostasis

26

1 1. Introduction

2 Obesity is a pandemic affecting nearly two billion people worldwide who also have significant increased
3 risk to comorbidities like type 2 diabetes (T2D) and its complications, cardiovascular disease and several
4 cancers [1]. Weight loss through lifestyle, diet and behavioural modification has poor compliance, with
5 the vast majority of patients relapsing in only a few years [2]. Conversely, bariatric surgeries, such as
6 Roux-en-Y gastric bypass (RYGB), confer sustained weight-loss and diabetes resolution [3, 4]. However,
7 bariatric surgeries are not a scalable solution to address the ever-increasing obesity burden. Thus, the
8 need for effective pharmacotherapies has driven intense investigation of the molecular mechanisms
9 underlying the efficacy of surgical intervention and has revealed a number of intriguing translatable
10 possibilities, namely the postprandial increase in circulating gut-derived hormones [5].

11 Glucagon-like peptide 1 (GLP-1), derived from differential proteolytic processing of proglucagon, and
12 PYY₃₋₃₆, generated by specific proteolysis of proPYY, are together secreted from intestinal L-cells in
13 response to nutrient intake. Both have emerged as leading pharmacological candidates for their potent
14 physiological effects to reduce food intake and induce weight loss [6]. GLP-1 mediated activation of
15 GLP-1 receptors (GLP-1R) on pancreatic β -cells potentiates glucose-induced insulin secretion and
16 maintains β -cell mass. Central activation of GLP-1Rs, particularly in the hypothalamus and hindbrain,
17 leads to delayed gastric emptying and inhibition of food intake, that when pharmacological GLP-1
18 analogues are applied can drive clinically relevant weight loss [7, 8]. The effects of PYY₃₋₃₆ have almost
19 exclusively been linked to central activation. PYY₃₋₃₆ can reduce food intake in both rodents and man,
20 and is thought to act via activation of the Neuropeptide Y Receptor Y2 (NPY2R) in the hypothalamus [9,
21 10]. Together, acute co-administration of PYY₃₋₃₆ and GLP-1-derived peptides render a synergistic
22 decrease in energy intake in obese men [11]. However, mechanistic details of the synergy between
23 these peptide agonists beyond food intake, body weight control and consequential effects on metabolic
24 homeostasis remain relatively scarce. In this study, we utilized long-acting analogues of GLP-1 and PYY₃₋₃₆
25 (via Fc-peptide conjugation) with submaximal doses to better characterize the synergistic
26 pharmacological benefits of their co-administration on body weight and glycaemic regulation in
27 obese/diabetic mouse models, and better outline the central neuronal circuitries by which they mediate
28 these effects.

29

30 2. Material and Methods

1 2.1 Compounds and cAMP accumulation assay

2 IgG1 Fc was generated with a cysteine substitution at position 442 (442C) in the CH3 domain using
3 standard DNA recombinant technologies [12] and expressed in CHO cells. The Y2R-selective peptide was
4 prepared by automated solid-phase synthesis using the Fmoc/^tBu protocol with a maleimide group at
5 lysine 11 to enable conjugation of the peptide to the free Cys (442C) in the Fc molecule. Crude peptides
6 were isolated by chromatography using an Agilent Polaris C8-A stationary phase (21.2 x 250 mm, 5
7 microns) eluting with a linear solvent gradient from 10% to 70% MeCN (0.1% TFA v/v) in water for 30
8 min using a Varian SD-1 Prep Star binary pump system, monitoring by UV absorption at 210 nm.
9 Following reduction and oxidation, the Fc was site specifically conjugated with the maleimide-
10 functionalized PYY₃₋₃₆ to yield Fc-PYY₃₋₃₆ (Figure 1C). The Fc-GLP-1R agonist was an internally-generated
11 (AstraZeneca, Gaithersburg, MD) version of Dulaglutide IgG4 Fc (exact same primary sequence) and was
12 purified as per Fc-PYY₃₋₃₆. Stable Chinese hamster ovary (CHO) cell lines overexpressing human or
13 mouse GLP-1R, NPY2R, and human NPY1R, NPY4R or NPY5R were generated at AstraZeneca using public
14 domain determined and confirmed sequences for each receptor. Half-maximal agonist potency
15 determinations (EC₅₀) for peptides inducing cAMP production were measured in the presence of 0.1%
16 BSA (Figure 2). cAMP generation was measured using the CisBio dynamic d2 cAMP HTRF assay kit
17 (CisBio, Codolet, France) according the manufacturer's guidelines as previously described [13, 14].
18 Cisplatin was purchased from Tocris Bioscience (Bristol, UK).

19 2.2 Experimental design

20 Animal studies were approved by either the Institutional Animal Care and Use Committee at
21 MedImmune/AstraZeneca (Gaithersburg, MD, USA) or Vanderbilt University (Nashville, TN, USA) in
22 accordance with Animal Welfare Act guidelines, or Gubra (Hørsholm, Denmark) under personal licenses
23 issued by the Danish Committee for Animal Research. Eight cohorts of group-housed male mice were
24 used in this study. Cohort A consisted of 8-week old C57BLKS/J *db/db* mice (Jackson Labs, Bar Harbor,
25 ME) used to assess the effects of Fc-GLP-1, Fc-PYY₃₋₃₆, and Fc-PYY₃₋₃₆ + Fc-GLP-1 on physiological
26 parameters and β -cell function. Cohort B consisted of 8-week old C57BLKS/J *db/db* mice (Jackson Labs)
27 used to assess the effect of Fc-PYY₃₋₃₆ + Fc-GLP-1 on energy expenditure and activity. Cohort C consisted
28 of 9-week old C57BLKS/J *db/db* and *db/+* mice (Jackson Labs) used to assess the effect of Fc-PYY₃₋₃₆ + Fc-
29 GLP-1 on insulin sensitivity and glucose disposal. Cohorts A-C were fed normal chow ad libitum prior to
30 and during the experiment, except in experiments including weight matched groups. In cohorts B and C

1 weight matching was achieved in C57BLKS/J *db/db* by pair feeding to match that consumed by the mice
2 administered Fc-PYY₃₋₃₆/GLP-1 the previous day and, if required, further reducing the pair fed amount by
3 5-15% to maintain weight matching to the Fc-PYY₃₋₃₆/GLP-1 group. Cohort D consisted of high fat diet
4 fed (Research Diets D12492, 8 weeks on diet) 18-week old C57BL6/J and Y2RKO mice (Jackson Labs, Bar
5 Harbor, ME, USA) used to assess the effect of Fc-PYY₃₋₃₆ + Fc-GLP-1 on insulin sensitivity and glucose
6 disposal. Constitutive Y2RKO mice (C57BL/6NTac-Npy2r^{em3978Tac}; Y2RKO) were generated at Taconic (San
7 Diego, CA) as described previously [15]. Cohort E consisted of 8-week old lean C57BL6/J, Y2RKO, and
8 Y2RKO/GLP-1RKO double knockout mice (Janvier Labs and Taconic, [16] used to assess the acute effect
9 of IP-injected Fc-GLP-1, Fc-PYY₃₋₃₆, and Fc-PYY₃₋₃₆ + Fc-GLP-1 combination on central cFOS reactivity 4h
10 post-dose. Cohort F consisted of 8-week old lean C57BL6/J mice (Janvier Labs, France) used to assess
11 the acute effect of IP-injected Fc-PYY₃₋₃₆ + Fc-GLP-1 on gene expression changes in the Area Postrema
12 (AP), Nucleus Tractus Solitarius (NTS), and ParaVentricular Nucleus (PVN) brain regions 4h post-dose.
13 Cohort G consisted of 8-week old lean C57BL6/J mice (Janvier Labs) used to assess the acute effect of IP-
14 injected Fc-GLP-1, Fc-PYY₃₋₃₆, and Fc-PYY₃₋₃₆ + Fc-GLP-1 on whole-brain cFOS reactivity 24-hours post-
15 dose. Cohort H consisted of 8-week old lean C57BL6/J mice (Janvier labs) used to assess conditioned
16 taste aversion to IP-injected Fc-GLP-1, Fc-PYY₃₋₃₆, and Fc-PYY₃₋₃₆ + Fc-GLP-1. All cohorts were
17 acclimatized for at least one week prior to study start. Cohorts A and B were randomized into groups
18 based on hemoglobin A1c levels (%HbA1c), while all other cohorts were randomized based on body
19 weight. Cohorts A, B, C, and D received Fc-GLP-1 (0.15 mg/kg SC, QAD), Fc-PYY₃₋₃₆ (1.0 mg/kg SC, QAD),
20 or Fc-PYY₃₋₃₆ + Fc-GLP-1 (0.3 mg/kg / 0.05 mg/kg SC, QAD dose escalated to 1.0mg/kg / 0.15 mg/kg after
21 one week). Cohorts E and F received Fc-GLP-1 (0.15 mg/kg IP), Fc-PYY₃₋₃₆ (1.0 mg/kg IP), or Fc-PYY₃₋₃₆ +
22 Fc-GLP-1 (1.0 mg/kg / 0.15 mg/kg IP) as indicated. Cohort G received Fc-GLP-1 (0.5 mg/kg IP), Fc-PYY₃₋₃₆
23 (1.0 mg/kg IP), or Fc-PYY₃₋₃₆ + Fc-GLP-1 (1.0 mg/kg / 0.5 mg/kg IP) as indicated. Cohort H received Fc-
24 GLP-1 (0.15 mg/kg SC), Fc-PYY₃₋₃₆ (1.0 mg/kg SC), Fc-PYY₃₋₃₆ + Fc-GLP-1 (1.0 mg/kg / 0.15 mg/kg SC), or
25 cisplatin (3 mg/kg SC). Phosphate-buffered saline (PBS) was used as vehicle control for all cohorts.
26 Animal care, use, and experimental protocols were approved by the institutional animal care and use
27 committees of AstraZeneca and Gubra.

28 2.3 *ipGTT and assay*

29 Six-hour fasted mice were injected intraperitoneally with 2.0 g/kg glucose in saline. Blood glucose was
30 determined at 0, 15, 30, 60, and 120 min. Plasma glucose was determined colorimetrically using glucose
31 oxidase kit (Cayman Chemical, Ann Arbor, MI). Plasma insulin levels were determined via ELISA

1 (MesoScale Discovery, Rockville, MD) in cohort A, and via RIA (MilliporeSigma, Temecular, CA) in cohorts
2 C and D. The HbA1c level was determined colorimetrically from whole blood (Crystal Chem Inc, Elk
3 Grove Village, IL).

4 *2.4 Islet and pancreas analysis*

5 Pancreatic insulin content was determined from whole pancreas using acid-ethanol extraction and
6 insulin ELISA. For immunohistochemistry, pancreata were fixed, embedded, and cut into 5 μm sections.
7 Insulin and glucagon staining, quantitation and analysis were performed all as previously described [17,
8 18]. Pancreatic islets from C57BL6/J or C57BLKS/J *db/db* mice were isolated by collagenase digestion as
9 previously described [19]. For qRT-PCR and transmission electron microscopy, freshly isolated islets
10 from C57BLKS/J *db/db* mice used. Transmission electron microscopy and quantitation of insulin
11 secretory granule numbers was performed as previously described [20]. qRT-PCR analysis was
12 performed using Taqman gene expression assay probe/primer sets (Thermo Fischer Scientific) for *Ins1*,
13 *Ins2*, *Gck*, *Pdx1*, *Slca2a*, and *Rna18s*; PrimePCR Probe Assay (Bio-Rad, Hercules, CA) was used for *Mafa*.
14 Results are shown as the target gene expression relative to *Rna18s* expression and normalized to vehicle
15 expression using the $2^{(-\Delta\Delta Ct)}$ method. For perfusion, freshly isolated islets from C57BLKS/J *db/db* mice
16 (Figure 2A-B) or overnight recovered islets (RPMI media, 10% FBS, 5.6 mmol/L glucose) from C57BL6/J
17 mice (Figure 2I-J) were used. Perfusion was performed as described previously [18]. For Figure 2I-J, Fc-
18 GLP-1 (100 nM), Fc-PYY₃₋₃₆ (1 μM) or the combination were added during the entire perfusion
19 procedure, as indicated.

20 *2.5 Energy expenditure*

21 Indirect calorimetry was performed with a Columbus Instruments Comprehensive Laboratory Animal
22 Monitoring System (CLAMS) (Columbus, OH). Cohort B consisted of 3 groups: C57BLKS/J *db/db* vehicle,
23 C57BLKS/J *db/db* Fc-PYY₃₋₃₆ + Fc-GLP-1 (dosed as described), and C57BLKS/J *db/db* weight matched to the
24 drug-treated group. Animals were dosed for 16 days; on day 12, animals were acclimated to the CLAMS
25 system for 48h. On day 14, respirometry and locomotor activity were monitored for 36h and recorded.

26 *2.6 Dual radiolabelled hyperinsulinemic-euglycemic clamp and glycogen assessment*

27 Clamp studies and associated calculations were performed as previously described [18, 21]. Cohort C
28 consisted of *db/+*, C57BLKS/J *db/db* vehicle, C57BLKS/J *db/db* Fc-PYY₃₋₃₆ + Fc-GLP-1, and C57BLKS/J *db/db*

1 weight-matched (WM) to the drug-treated group. Cohort D consisted of DIO C57BL6/J vehicle, DIO
2 C57BL6/J Fc-PYY₃₋₃₆ + Fc-GLP-1, DIO Y2RKO vehicle, and DIO Y2RKO Fc-PYY₃₋₃₆ + Fc-GLP-1 mice (D12492,
3 Research Diets). In both cohorts C and D, animals were dosed SC QAD for 1 week with low dose
4 compound. Jugular vein and carotid artery catheters were placed 7 days prior to the experiment.
5 Animals were then dosed SC QAD for an additional week with high dose compound. On the day of the
6 clamp study conscious, unrestrained 5h fasted mice under were simultaneously infused into the jugular
7 vein with a constant rate of 0.1 $\mu\text{Ci}/\text{mi}$ [³H]-glucose. After a basal period, a variable rate 20% dextrose to
8 maintain target glycemia, and a constant rate of human insulin were infused into the jugular vein
9 catheter. Arterial blood samples were taken over 10 min from the arterial catheter and the glucose
10 infusion rate was adjusted to maintain the glucose at a target concentration. For cohort C (N \geq 6/group),
11 steady state glucose was achieved at 200 mg/dL using 40mU/min/kg (lean mass) of insulin. For cohort D
12 (N \geq 7/group), steady state glucose was achieved at 110 mg/dL using 4mU/min/kg (body weight) of
13 insulin. At 120 min, a bolus of [¹⁴C]-2-deoxy-glucose was infused to assess tissue-specific glucose
14 uptake. At 155 min, animals were sacrificed with pentobarbital anaesthesia and tissues were collected.
15 Total glycogen content and tracer- determined glycogen synthesis in gastrocnemius and liver were
16 assessed as described previously [22].

17 2.7 Conditioned taste aversion

18 One week prior to assessment, animals were single-housed with *ad libitum* access to food and one
19 bottle of water. The position of the water bottle was switched daily to minimize the development of
20 side preference. The animals were weighed and handled daily 3 days prior to assessment. On the day
21 of conditioning and following 12h of water deprivation (day 1), animals were exposed to a bottle
22 containing highly palatable 0.1% saccharin flavoured water (4 h access). Immediately after (t = 0h),
23 animals were IP-dosed with Fc-PYY₃₋₃₆, Fc-GLP-1, Fc-PYY₃₋₃₆ + Fc-GLP-1 or cisplatin, as indicated. Seventy-
24 two hours later, a voluntary choice between tap water and 0.1% saccharin solution was provided, and
25 both water and saccharin solution intake were measured after 24h (i.e., between t = 72h and 96h).

26 2.8 cFOS quantitation

27 Animals from cohort E were IP-sham dosed for 3 days prior to termination. On the study day, animals
28 were dosed IP with compound as indicated, sacrificed via midazolam anaesthesia followed by isoflurane
29 inhalation 4h post-dose, transcardially perfused with heparinized saline (15,000 IU/L) followed by 4%
30 paraformaldehyde for 5 min (10 mL/min) and brains removed 4h following IP-dosing. Brains were

1 removed, post-fixed overnight in the same fixative and transferred for 2 days to a 30% sucrose solution.
2 Brains were cut into six series of 40 μm coronal sections on a freezing microtome and stored until
3 immunohistochemical processing. cFOS immunostaining and counting of c-FOS positive cell nuclei were
4 performed as previously described [23]. An initial qualitative cFOS screen was performed in lean
5 C57BL6/J mice following the above procedure to identify regions of interest for c-FOS quantitation (data
6 not shown).

7 *2.9 Laser capture microdissection and RNAseq-bioinformatics*

8 Laser capture microdissection was performed as previously described [24, 25] on brains from cohort F
9 4h following IP-dosing. Briefly, snap-frozen brains were sectioned (10 μm thickness) on a Cryostat
10 (model CM350 S, Leica Biosystems, Nussloch, Germany). Sections were collected onto PEN membrane
11 glass slides (Thermo Fischer Scientific), fixed, crystal violet stained and dehydrated. LCM was performed
12 using an ArcturusXT microdissection system (Thermo Fischer Scientific). A combination of the infrared
13 capture laser and the ultraviolet cutting laser allowed the isolation of 4 mm^2 tissue from each brain
14 region per animal. RNA was isolated using the PicoPure RNA isolation kit (Thermo Fischer
15 Scientific). RNAseq libraries were prepared with NeoPrep using the Illumina TruSeq stranded mRNA
16 library kit for NeoPrep and sequenced (75 base pair single-end reads) on the NextSeq 500 (Illumina, San
17 Diego, CA). Reads were aligned to the GRCm38 v89 Ensembl *Mus musculus* genome using STAR v.2.5.2a
18 [26]. Differential gene expression analysis was performed with the R package DESeq2 [27], and genes
19 were considered significantly regulated based on having a false discovery rate (FDR) less than 0.01. A
20 gene set analysis was conducted with the R package Piano [28] using the Stouffer method. The gene sets
21 were defined based on the Reactome pathway database [29], and gene sets smaller than 4 genes were
22 excluded from the analysis. The data discussed in this publication have been deposited in NCBI's Gene
23 Expression Omnibus [24, 25] and are accessible through GEO Series accession number GSE160802. Gene
24 sets were considered significantly enriched based on having a Benjamini-Hochberg corrected *p*-value
25 less than 0.01.

26 *2.10 Light Sheet Microscopy*

27 Twenty four hours following IP-dosing, animals in cohort G were anesthetized with a mixture of
28 Hypnorm (Glostrup Pharmacy, Denmark) and Dormicum (Hameln Pharma, Germany) and then perfused
29 with heparinized (15,000 IU/L) PBS followed by 10% neutral buffered formalin (NBF). Brains were then
30 removed, post-fixed overnight at room temperature in NBF, washed in PBS, methanol dehydrated (20%,

1 40%, 60%, 80% and 100%, 1h each at room temperature), and stored in 100% methanol until whole
2 brain immunohistochemistry, which was accomplished with a modified version of the iDISCO protocol
3 [30]. Permeabilization was carried out at 37°C for 3 days, blocking at 37°C for 2 days and antibody
4 labelling with primary anti-cFOS antibody (Cell Signaling Technology, US; cat no #2250;
5 RRID:AB_2247211) at 37°C for 7 days. Samples were washed and incubated with secondary antibody
6 (donkey-anti-Rb_Cy-5, Jackson ImmunoResearch, UK; cat no #711-175-152; RRID:AB_2340607) at 37°C
7 for 7 days. Brains were then dehydrated in methanol/water series and cleared using 66%
8 dichloromethane/33% methanol for 3h, then 100% dichloromethane 2 x 15 min, and finally transferred
9 to dibenzyl ether in closed glass vials.

10 Brains were imaged using a Lavisision light sheet ultramicroscope II (Miltenyi Biotec GmbH, Bergisch
11 Gladbach, Germany)) with Zyla 4.2P-CL10 sCMOS camera (Andor Technology, Belfast, United Kingdom),
12 SuperK EXTREME supercontinuum white-light laser EXR-15 (NKT photonics, Birkerød, Denmark) and MV
13 PLAPO 2XC (Olympus, Tokyo, Japan) objective. The brain was attached to transparent sample holder
14 made of silicone with neutral silicone gel (ventral side up) and imaged in a chamber filled with DBE.
15 Inspector microscope controller software (v7) was used (Miltenyi Biotec GmbH, Bergisch Gladbach,
16 Germany). Horizontal images were acquired at 0.63x magnification (1.2x total magnification) with an
17 exposure time of 254 ms in a z-stack at 10 μ m intervals. Horizontal focusing was captured in 9 planes
18 with blending mode set to the center of the image to merge the individual raw images.
19 Autofluorescence images were captured at 560 \pm 20 nm (excitation) and 650 \pm 25 nm (emission)
20 wavelength (80% laser power in Inspector software, 100% NKT laser). cFOS staining was imaged at 630
21 \pm 15 nm excitation wavelength and 680 \pm 15 nm emission wavelength (100% laser power in software,
22 100% mechanical). Samples were scanned in random order using identical settings.

23 Images were reconstructed to create a 3-D image of the entire brain and aligned to Allen's CCFv3 brain
24 atlas [31]. To determine the difference in cFOS positive cells between light sheet microscopy samples, a
25 negative binomial generalized linear model was fitted to the data. Deviance residuals of the statistical
26 model were investigated to ensure alignment with assumptions of normality and homoscedasticity.
27 Cook's distance was calculated for each data point to ensure that no data point overly influenced the
28 model.

29
30 *2.11 Statistics*

1 Data normality was determined by the D'Agostino and Pearson Test. Parametric data were analysed by
2 Student's t-test for 2 groups, or one or two-way ANOVA followed by Tukey's or Sidak's post-hoc test for
3 > 2 groups. Non-parametric data were analysed by Mann-Whitney test for 2 groups, or Kruskal-Wallis
4 test followed by Dunn's post-hoc test for > 2 groups. Data are presented as mean \pm SE of at least 3
5 biological replicates (with the exception of Figure 6F, WT, GLP-1 where only N=2 was available due to
6 technical error). All data were analysed using GraphPad Prism 7.02 (GraphPad, San Diego, CA).
7 Statistical significance was set at $p \leq 0.05$. Indirect calorimetry data were analysed by CalR [31, 32] using
8 a general linear model based on ANCOVA.

9 **3. Results**

10 *3.1 Fc-PYY₃₋₃₆ and Fc-GLP-1 generation*

11 Recombinant IgG1 Fc was generated with a cysteine substitution at position 442 (442C) of the CH3
12 domain using standard DNA recombinant technologies [12] and expressed in CHO cells (Supplementary
13 Figure 1A). The Synthetic Y2R-selective peptide was prepared by automated solid-phase synthesis with a
14 maleimide functional group at Lysine 11 (Supplementary Figure 1B). Following reduction and
15 oxidation, the maleimide-functionalized PYY₃₋₃₆ was site specifically conjugated to the Fc molecule at
16 position 442C to yield Fc-PYY₃₋₃₆ (Supplementary Figure 1C). Further detail is provided in the methods
17 section. The Fc-GLP-1R agonist was an internally generated (AstraZeneca, Gaithersburg, MD) version of
18 Dulaglutide IgG4 Fc and was purified as per Fc-PYY₃₋₃₆. Stable Chinese hamster ovary (CHO) cell lines
19 overexpressing human or mouse GLP-1R or Y2R were used for assessment of half-maximal agonist
20 potency (EC₅₀) for inducing cAMP production (Supplementary figure 1D, 1E). Fc-GLP-1 showed EC₅₀ 12.8
21 \pm 2.0 pM and 41.3 \pm 6.0 pM and Fc-PYY₃₋₃₆ EC₅₀ 1.3 \pm 0.3 pM and 2.8 pM in human and mouse,
22 respectively. Fc-PYY₃₋₃₆ was highly specific to Y2R over Y1R, Y4R and Y5R by at least 10,000-fold (data not
23 shown).

24 *3.2 Fc-PYY₃₋₃₆ promotes diabetes remission in combination with Fc-GLP-1 in C57BLKS/J db/db mice*

25 Eight-week old C57BLKS/J *db/db* mice were treated with Fc-PYY₃₋₃₆, Fc-GLP-1, or Fc-PYY₃₋₃₆ + Fc-GLP-1 for
26 4 weeks. We selected sub-maximal doses when administered as monotherapies (Fc-PYY₃₋₃₆ 1 mg/kg and
27 Fc-GLP-1 0.15 mg/kg) to maximize the window of opportunity to observe the synergistic potential of
28 combination treatment. Body weights were unchanged between monotherapy and vehicle-treated
29 animals but were significantly reduced by 7% in Fc-PYY₃₋₃₆ + Fc-GLP-1 versus vehicle-treated mice (Figure
30 1A, 1B). Vehicle-treated animals displayed an \sim 4-point increase in %HbA1c which was significantly

1 mitigated by both monotherapy treatments, while Fc-PYY₃₋₃₆ + Fc-GLP-1 treatment led to a 0.7-point
2 reduction in %HbA1c over the study period, that amounted to an ~5-point decrease in %HbA1c relative
3 to the vehicle control (Figure 1C). At week 3 of treatment, glucose tolerance was unchanged with either
4 monotherapy treatment, but was significantly improved in the Fc-PYY₃₋₃₆ + Fc-GLP-1 combination group
5 (Figure 1D) amounting to a 33% reduction in glucose AUC (Figure 1E). Fasting plasma blood glucose was
6 not different after Fc-PYY₃₋₃₆ or Fc-GLP-1 treatment versus vehicle (control), however the combination of
7 Fc-PYY₃₋₃₆ + Fc-GLP-1 significantly reduced plasma glucose by ~66% (Figure 1F). The decreased fasting
8 plasma glucose levels were paralleled by corresponding increases in fasting insulin levels, for both Fc-
9 GLP-1 and Fc-PYY₃₋₃₆ + Fc-GLP-1 (Figure 1G). Pancreatic insulin content was unchanged at termination by
10 monotherapy treatment but was strongly increased by Fc-PYY₃₋₃₆ + Fc-GLP-1 combination treatment by
11 over 8-fold (Figure 1H), implicating possible enhanced β -cell function and/or mass as a contributor to
12 the synergistic improvement in metabolic homeostasis induced by peptide co-administration.

13 As such, primary pancreatic islets were isolated from vehicle and Fc-PYY₃₋₃₆ + Fc-GLP-1 treated animals.
14 Islets were subjected to dynamic perfusion with 2.8 mM glucose (basal) for 40 min followed by 16.7
15 mM glucose (stimulatory) for 50 min (Figure 2A). Islets from combination-treated animals displayed >6-
16 fold increase in first phase insulin secretion, and >7-fold increase in second phase insulin secretion,
17 implicating a marked recovery in β -cell insulin secretory capacity (Figure 2B). Expression of key genes
18 related to β -cell function, including *Ins1*, *Ins2*, *Gck*, *Sica2a*, *Pdx1*, and *Mafa* were all significantly
19 increased in islets from combination-treated versus vehicle-treated mice (Figure 2C). Electron
20 micrograph analysis of β -cells from vehicle-treated mice indicate a dramatic decrease of the mature
21 insulin secretory granule population and expansion of the rough endoplasmic reticulum/Golgi apparatus
22 compartments (Figure 2D), while Fc-PYY₃₋₃₆ + Fc-GLP-1-treated animals exhibited a recovery of insulin
23 secretory granule numbers and normalized morphology of other organelles (Figure 2E). This is
24 consistent with previous studies of physiological and pharmacological restoration of β -cell function [17,
25 18, 20]. Image quantification indicated the number of mature insulin secretory granules per β -cell
26 cytoplasmic area was increased by over 5-fold in Fc-PYY₃₋₃₆ + Fc-GLP-1-treated animals (Figure 2F),
27 paralleling the enhancement in total pancreatic insulin content. The population of immature insulin
28 secretory granules was also reduced by Fc-PYY₃₋₃₆ + Fc-GLP-1, supporting improved functional capacity in
29 these treated islet β -cells (Figure 2G). Additional representative electron micrographs are also shown
30 (Supplementary Figure 2), as further evidence of the adaptive plasticity of pancreatic β -cells and
31 restoration of the mature insulin secretory granule store by Fc-PYY₃₋₃₆ + Fc-GLP-1-treatment.

1 Morphometric analysis of insulin and glucagon immunohistochemical co-stained sections indicated
2 unaltered pancreatic α -cell mass but an apparent increase in pancreatic β -cell mass, as assessed by
3 insulin positive staining, in Fc-PYY₃₋₃₆ + Fc-GLP-1-treated animals (Figure 2H). Representative images of
4 pancreatic islets (Supplementary Figure 3), indicate little change in β -cell proliferation as previously
5 observed (Boland et al, 2019b), and more intensive insulin and MafA staining complementary to
6 increased pancreatic islet insulin content (Figures 2H and 2D-G) and *MafA* gene expression (Figure 2C).
7 To exclude a direct effect of Fc-PYY₃₋₃₆ on islets, overnight cultured primary islets from naïve C57BL6/J
8 mice were subjected to perfusion at basal (2.8 mM) and stimulatory (16.7 mM) glucose in the presence
9 of Fc-GLP-1 (100 nM), Fc-PYY₃₋₃₆ (1 μ M) or the combination (Figure 2I). As expected, Fc-GLP-1
10 potentiated glucose-stimulated insulin secretion, however Fc-PYY₃₋₃₆ had no effect alone and did not
11 enhance the Fc-GLP-1 response (Figure 2J).

12 *3.3 Fc-PYY₃₋₃₆ + Fc-GLP-1 does not affect RER but reduces total activity and VO₂*

13 To identify physiological changes that could account for the weight loss and improvements in glucose
14 homeostasis induced by Fc-PYY₃₋₃₆ + Fc-GLP-1 combination treatment, indirect calorimetry assessment of
15 C57BLKS/J *db/db* mice treated with vehicle, Fc-PYY₃₋₃₆ + Fc-GLP-1, or vehicle and weight-matched (WM)
16 to Fc-PYY₃₋₃₆ + Fc-GLP-1-treated mice via food restriction was conducted. Vehicle-treated mice gained
17 weight throughout the study period, while both Fc-PYY₃₋₃₆ + Fc-GLP-treated and WM controls lost
18 approximately 15% of body weight at the time of indirect calorimetry (Figure 3A, 3B). VO₂ was reduced
19 in Fc-PYY₃₋₃₆ + Fc-GLP-1-treated and WM animals relative to the controls during both light and dark
20 phases, but this effect was more pronounced during dark phase in WM mice (Figure 3C, 3D). The
21 respiratory exchange ratio (RER) was reduced in WM animals but increased by Fc-PYY₃₋₃₆ + Fc-GLP-1
22 treatment during dark phase (Figure 3E). Energy expenditure was reduced in both Fc-PYY₃₋₃₆ + Fc-GLP-1-
23 treated and WM animals compared to *db/db* but energy expenditure was increased in Fc-PYY₃₋₃₆ + Fc-
24 GLP-1-treated animals compared to WM animals (Figure 3F). Total physical activity was decreased
25 during both light and dark phases in Fc-PYY₃₋₃₆ + Fc-GLP-1-treated animals but only during the dark phase
26 in WM controls (Figure 3G). Common side effects of GLP-1 and Fc-PYY₃₋₃₆ agonism include nausea
27 (Bettge 2017) and emesis [33], respectively. Therefore, we assessed the potential for an aversive
28 response to Fc-GLP-1, Fc-PYY₃₋₃₆ and the combination in naïve lean C57BL6/J mice using a conditioned
29 saccharin preference test. All animals demonstrated similar saccharin intake prior to dosing
30 (Supplementary Figure 4A), and all compounds induced weight loss following acute administration
31 (Supplementary Figure 4B, 4C). Over a 24 h period following compound administration (72-96 h post-

1 dose), total fluid intake was significantly reduced in groups receiving cisplatin (positive control) and Fc-
2 GLP-1 (Supplementary Figure 4D). Water intake was significantly increased in all treatment groups
3 (Supplementary Figure 4E). Saccharin intake, saccharin preference and the consumed saccharin to
4 water ratio were all significantly reduced by cisplatin and Fc-PYY₃₋₃₆ + Fc-GLP-1 (Supplementary Figure
5 4F, 4G, 4H). These data indicate that the combination of Fc-PYY₃₋₃₆ + Fc-GLP-1 induces a greater degree
6 of aversive behaviour than either monotherapy.

7 *3.4 Fc-PYY₃₋₃₆ + Fc-GLP-1 improves insulin sensitivity and hepatic glycogen synthesis independent of* 8 *weight loss in C57BLKS/J db/db mice*

9 To explore weight-independent mechanisms of Fc-PYY₃₋₃₆ + Fc-GLP-1 on insulin action, a
10 hyperinsulinemic-euglycemic clamp in severely insulin resistant obese/diabetic C57BLKS/J *db/db* mice
11 treated with vehicle or Fc-PYY₃₋₃₆ + Fc-GLP-1 for 2 weeks was performed. Control groups consisted of
12 C57BLKS/J *db/db* mice weight matched (WM) to the Fc-PYY₃₋₃₆ + Fc-GLP-1 group and lean C57BLKS/J *db/+*
13 mice. *Db/+* mice were much lighter than their *db/db* counterparts with Fc-PYY₃₋₃₆ + Fc-GLP-1
14 administration inducing a 14% body weight reduction over the 2-week period, and WM-controls
15 exhibited similar reductions (Figure 4A, Supplementary Figure 5A). In consideration of divergent starting
16 blood glucose concentrations (121 mg/dL in C57BLKS/J *db/+* mice versus 404 mg/dL in C57BLKS/J *db/db*
17 mice in the basal period t=-10 to 0 min; Figure 4B; Supplementary Figure 5B), glucose levels were
18 clamped at 200 mg/dL with glucose stabilized between groups by 60 min of clamp (Figure 4B). Fc-PYY₃₋₃₆
19 + Fc-GLP-1 led to ~20-fold increase in the glucose-infusion rate (GIR) versus vehicle *db/db* animals,
20 which was significantly higher than WM controls, indicating weight loss-independent effects of Fc-PYY₃₋₃₆
21 + Fc-GLP-1 on enhanced insulin sensitivity (Figure 4C), although the possibility of an altered weight-
22 dependence to insulin sensitivity cannot be ruled out. Basal insulin levels were elevated in *db/db* mice
23 compared to *db/+* and reduced by Fc-PYY₃₋₃₆ + Fc-GLP-1-treated animals compared with WM controls
24 (Figure 4D). During insulin-infusion (i.e. clamp) period insulin levels were not different between groups
25 (Figure 4D). Using tracer approaches, we assessed the impact on hepatic and extrahepatic glucose
26 metabolism. Basal whole-body glucose disposal (Rd; Figure 4E) and hepatic glucose production (Ra;
27 Figure 4F) were both significantly reduced by Fc-PYY₃₋₃₆ + Fc-GLP-1 treatment compared with vehicle and
28 is reflective of reduced basal whole-body glucose turnover contributing to the decrease in basal glucose
29 levels (Figure 4B and Supplementary Figure 5B). Under insulin-stimulated conditions, Rd was strongly
30 increased in *db/+* mice compared to *db/db* vehicle. Both WM and Fc-PYY₃₋₃₆ + Fc-GLP-1 groups increase
31 Rd compared to vehicle-treated animals and Fc-PYY₃₋₃₆ + Fc-GLP-1 was further enhance compared with

1 WM consistent with the observed increase in glucose infusion rate (Figure 4E). Fc-PYY₃₋₃₆ + Fc-GLP-1
2 treatment shifted the relationship observed between Rd and circulating insulin levels to the left (i.e.
3 increased insulin sensitivity) toward that seen in lean controls, but was not seen in the WM group
4 (Supplementary Figure 5C). During the clamp period insulin trended to suppressed endogenous glucose
5 production (EGP) more so with Fc-PYY₃₋₃₆ + Fc-GLP-1 treatment as compared with WM and vehicle-
6 treated animals ($p=0.08$; Figure 4F) despite similar insulin levels (Supplementary Figure 5D). To
7 determine the site for the enhancement in peripheral glucose disposal we assessed tissue specific
8 glucose uptake (Rg). Tissue-specific glucose uptake was enhanced in all db/+ tissues evaluated compared
9 with db/db vehicle (Figure 4G, H). Fc-PYY₃₋₃₆ + Fc-GLP-1 treatment enhanced skeletal muscle
10 (gastrocnemius, vastus and soleus) and cardiac glucose uptake to levels compared with db/db vehicle
11 and WM mice (Figure 4G, 5H). WM mice demonstrated increased brown adipose tissue glucose uptake
12 compared with vehicle only (Figure 4H). As the clamps were performed at a mild hyperglycemia (200
13 mg/dl), which could augment hepatic glycogen synthesis; we assessed the core glycogen stores as well
14 as tracer-determined (direct) glycogen synthesis. Core hepatic glycogen was increased in db/db vehicle
15 compared to lean db/+ mice, which is consistent with their basal hyperglycemia and trended towards
16 being reduced by WM ($p=0.056$; Figure 4I). Fc-PYY₃₋₃₆ + Fc-GLP-1 dramatically increased insulin
17 stimulated hepatic glycogen synthesis (Figure 4J). In contrast with the liver, core and insulin-stimulated
18 skeletal muscle glycogen synthesis were significantly reduced in db/db mice compared with db/+ and
19 were not increased by Fc-PYY₃₋₃₆ + Fc-GLP-1 combination or WM (Figure 4K, 4L).

20 *3.5 Fc-PYY₃₋₃₆ + Fc-GLP-1 enhancement of hepatic glycogen synthesis, but not skeletal muscle glucose* 21 *uptake, requires Y2R agonism in diet-induced obese (DIO) mice*

22 To better characterize the contribution of the GLP-1R to Fc-PYY₃₋₃₆ + Fc-GLP-1 pharmacology,
23 hyperinsulinemic-euglycemic clamps were performed in DIO WT and Y2RKO mice to examine the
24 impact of Fc-PYY₃₋₃₆ + Fc-GLP-1 dual agonism on insulin action. Body weight loss and reduced fasting
25 glucose induced by Fc-PYY₃₋₃₆ + Fc-GLP-1 dual agonism was blunted in Y2RKO versus WT mice (14% vs
26 32%, body weight respectively) (Figure 5A, Supplementary Figure 6A). Fasting glucose was reduced by
27 Fc-PYY₃₋₃₆ + Fc-GLP-1 in both WT and Y2RKO with a significantly greater magnitude in WT mice (Figure 5B
28 and Supplementary 6B). Glucose was clamped at 110 mg/dL and was stabilized between groups by 30
29 min of insulin infusion (Figure 5B). GIR was significantly increased by Fc-PYY₃₋₃₆ + Fc-GLP-1 dual agonism
30 in both genotypes compared with their respective vehicle groups and was further increased in in WT Fc-
31 PYY₃₋₃₆ + Fc-GLP-1 vs. Y2RKO Fc-PYY₃₋₃₆ + Fc-GLP-1 mice from 80-110 min (Figure 5C). Basal insulin levels

1 were significantly decreased by Fc-PYY₃₋₃₆ + Fc-GLP-1 dual agonism WT and Y2RKO mice compared with
2 their respective vehicle controls (Figure 5D). Under clamp conditions, WT mice administered the Fc-
3 PYY₃₋₃₆ + Fc-GLP-1 combination demonstrated significantly reduced insulin levels compared to the WT
4 vehicle (Figure 5D), despite equal concentration of insulin infusion. A minor limitation of this experiment
5 is the absence of C-peptide analysis to better elucidate the contribution of endogenous insulin secretion
6 vs. insulin clearance in this effect. Basal whole-body glucose disposal was not different between groups,
7 but was significantly and similarly increased in both WT and Y2RKO mice administered Fc-PYY₃₋₃₆ + Fc-
8 GLP-1 combination (Figure 5E), with a clear relationship between circulating insulin levels and whole-
9 body glucose disposal was observed (Supplementary Figure 6C). These data indicate that the presence
10 of Y2R signalling played a minor role in the insulin sensitizing effects of Fc-PYY₃₋₃₆ + Fc-GLP-1 dual
11 agonism and GLP-1R signalling was sufficient to maximize the insulin sensitizing effect. Basal hepatic
12 glucose production (Ra) was not different between groups (Figure 5F). During the clamp, hepatic glucose
13 production was equally suppressed in WT mice regardless of treatment (Figure 5F). However, Ra was
14 elevated in Y2RKO vehicle compared with WT vehicle, and this was significantly reduced Fc-PYY₃₋₃₆ + Fc-
15 GLP-1 treatment in Y2RKO mice (Figure 5F). The suppression of hepatic glucose production during clamp
16 conditions in Fc-PYY₃₋₃₆ + Fc-GLP-1 treated mice showed an improved relationship with circulating insulin
17 levels by a shift of the curve to the left and steeper slope suggesting improved hepatic insulin sensitivity
18 (Supplementary Figure 6D). Similar to the findings in C57BLKS/J *db/db* mice, there was a trend for a
19 treatment effect of Fc-PYY₃₋₃₆ + Fc-GLP-1 dual agonism to increase skeletal muscle (gastric and vastus)
20 glucose uptake, albeit not significant (Figure 5G). However, Fc-PYY₃₋₃₆ + Fc-GLP-1 administration
21 significantly increased brown adipose tissue and decrease cardiac glucose uptake in WT mice (Figure
22 5H). Core hepatic glycogen levels were significantly increased in Y2RKO mice administered Fc-PYY₃₋₃₆ +
23 Fc-GLP-1 compared with Y2RKO vehicle (Figure 5I). Insulin-stimulated hepatic glycogen synthesis was
24 significantly increased in WT mice administered Fc-PYY₃₋₃₆ + Fc-GLP-1 compared with WT vehicle (Figure
25 5J). Core skeletal muscle glycogen levels were significantly increased in Y2RKO versus WT mice when
26 both were administered Fc-PYY₃₋₃₆ + Fc-GLP-1 (Figure 5I), and skeletal muscle insulin-stimulated glycogen
27 synthesis was significantly increased in Y2RKO mice administered Fc-PYY₃₋₃₆ + Fc-GLP-1 compared with
28 Y2RKO vehicle (Figure 5J).

29 *3.6 Fc-PYY₃₋₃₆ + Fc-GLP-1 activates discrete hypothalamic and brainstem nuclei following acute*
30 *administration*

1 This physiological data indicated that a putative mechanism for the metabolic effects of a Fc-PYY₃₋₃₆ + Fc-
2 GLP-1 combination could be increased insulin sensitivity in liver and perhaps skeletal muscle. As neither
3 *Glp1r* nor *Npy2r* are expressed in these tissues (GEO datasets, NCBI), we excluded direct action in these
4 tissues as a mechanism for the efficacy of Fc-PYY₃₋₃₆ + Fc-GLP-1 treatment. More likely, the role of the
5 central nervous system (CNS), particularly the hypothalamus, in regulating appetite, body weight,
6 energy expenditure, and metabolic homeostasis influences insulin sensitivity. As such, a qualitative
7 screen of cFOS activation (as a surrogate marker of neuronal activation) throughout the brain of lean
8 C57BL6/J mice 4 h following single administration of Fc-GLP-1, Fc-PYY₃₋₃₆, or Fc-PYY₃₋₃₆ + Fc-GLP-1 was
9 conducted. Furthermore, to better define the contribution of *Npy2r* and *Glp1r* to the activation of cFOS
10 under the same treatments, we acutely dosed naïve lean Y2RKO, and Y2RKO/GLP-1RKO double knockout
11 mice [16] and performed the same analysis (Figure 6 and Supplementary Figure 7). cFOS expression in
12 the central nucleus of the amygdala (CeA) was strongly induced by Fc-GLP-1, and loss of Y2R had no
13 effect on the magnitude of the cFOS response in either Fc-GLP-1 or Fc-PYY₃₋₃₆ + Fc-GLP-1 administered
14 animals, indicating that the effect was solely dependent on the GLP-1R (Figure 6A). Somewhat
15 surprisingly, neither the arcuate nucleus (ARC) nor the ventromedial hypothalamic nucleus (VMH) were
16 activated by Fc-GLP-1 or Fc-PYY₃₋₃₆ + Fc-GLP-1, which may be a consequence of assessing cFOS 4 h after
17 administration rather than an earlier timepoint (Figure 6B, 6C). The bed of the stria terminalis (BST) was
18 significantly activated by both Fc-GLP-1 and Fc-PYY₃₋₃₆, but no additive effect of the combination was
19 observed (Figure 6D). Loss of Y2R blunted both Fc-GLP-1 and Fc-PYY₃₋₃₆-monotherapy mediated
20 activation, but the combination maintained a similar response as that observed in WT animals (Figure
21 6D). The parabrachial nucleus (PBN) tended to be activated by monotherapy administration of either Fc-
22 PYY₃₋₃₆ or Fc-GLP-1, but was significantly increased by Fc-PYY₃₋₃₆ + Fc-GLP-1 ($p < 0.0001$). Loss of Y2R did
23 not affect the magnitude of the cFOS response of Fc-GLP-1, alone or in combination with Fc-PYY₃₋₃₆,
24 indicating exclusive GLP-1R mediation of the observed effect (Figure 6E). While Fc-PYY₃₋₃₆ alone had no
25 effect in the area postrema (AP), some interaction was observed when administered in combination
26 with Fc-GLP-1 (Figure 6F). Both the nucleus of the solitary tract (NTS) and the paraventricular nucleus of
27 the hypothalamus (PVN) demonstrated increased cFOS activation following either Fc-PYY₃₋₃₆ or Fc-GLP-1
28 monotherapy administration, although this only achieved significance in the NTS following Fc-PYY₃₋₃₆
29 monotherapy administration (Figure 6G, 6H). However, marked synergistic cFOS activation following Fc-
30 PYY₃₋₃₆ + Fc-GLP-1 administration, which was strongly blunted in animals lacking Y2R, was evident in both
31 the NTS and PVN, implicating both the hindbrain and the hypothalamus as putative mediators of the
32 early synergistic action of Fc-PYY₃₋₃₆ + Fc-GLP-1 (Figure 6G, 6H).

1 To further characterize the early transcriptomic changes induced by Fc-PYY₃₋₃₆ + Fc-GLP-1 co-agonism,
2 we utilized laser capture microdissection to isolate the NTS, ARC, and PVN from lean C57BL6/J mice 4 h
3 following compound co-administration and performed RNA sequencing. Principal component analysis
4 (PCA) revealed segregation by brain region but not co-agonist administration (Supplementary Figure
5 8A). Fc-PYY₃₋₃₆ + Fc-GLP-1 co-administration led predominantly to down-regulation of gene expression in
6 all regions, with the PVN showing the most abundant number of differentially up- and down-regulated
7 genes versus the ARC and NTS (Supplementary Figure 8B). Reactome database analysis revealed
8 significant regulation by Fc-PYY₃₋₃₆ + Fc-GLP-1 combination in the NTS of several potential metabolic and
9 signalling pathways (Supplementary Figure 8C), but the ARC did not demonstrate any significantly
10 regulated gene sets at the cut-off of $p < 0.01$. From this analysis, we provide the relative gene
11 expression levels (z-scores) of significantly up- or down-regulated genes (Supplementary Figure 8D).
12 Numerous genes related to energy metabolism and growth, including *FoxO1*, *Btg2*, *Socs3*, and *Sdc4*,
13 were found to be highly regulated in the PVN, as well as genes associated with neuronal plasticity and
14 development, including *Sdc4*, *Hs3st1*, and *Hs3st2*.

15 As the early (4 h) synergistic activation of appetite-regulating neurons in the hypothalamus and
16 hindbrain likely initiates the cascade of pro-metabolic effects exerted by Fc-PYY₃₋₃₆ + Fc-GLP-1
17 combination, we next examined global cFOS reactivity 24 h following acute monotherapy and co-agonist
18 administration to better indicate downstream neuronal activity and to identify a putative functional link
19 between neuronal activation and physiological effects of Fc-PYY₃₋₃₆ + Fc-GLP-1 co-administration.
20 Fluorescent light sheet microscopy analysis of whole-brains from lean C57BL6/J mice 24 h following Fc-
21 PYY₃₋₃₆, Fc-GLP-1, or Fc-PYY₃₋₃₆ + Fc-GLP-1 combination revealed that most of the hypothalamic and
22 hindbrain areas of the brain that were significantly activated at 4 h by co-agonist administration were
23 largely unaffected at 24 h. Both the CeA and PBN showed significantly increased cFOS reactivity
24 following Fc-PYY₃₋₃₆ + Fc-GLP-1 co-administration, although the magnitude of activation was markedly
25 reduced versus that observed at 4 h (Figure 7A, 7E). The ARC was not significantly activated, although a
26 clear trend towards increased cFOS reactivity due to Fc-GLP-1 was present (Figure 7B). Similarly, the
27 BST, AP and PVN were not significantly activated by a Fc-PYY₃₋₃₆ + Fc-GLP-1 combination, although a
28 trend towards activation by Fc-GLP-1 in the AP and BST was observed (Figure 7D, 7F, 7H). Interestingly,
29 the dorsal motor nucleus of the vagus nerve (DMX), which resides in the medulla and is an area of the
30 brain that was seemingly unaffected, and therefore not quantified at 4 h, was the most markedly
31 activated region 24 h post Fc-PYY₃₋₃₆ + Fc-GLP-1 co-agonist administration (Figure 7C). The clear

1 synergistic activation of cFOS in the NTS by Fc-PYY₃₋₃₆ + Fc-GLP-1 combination observed at 4 h remained
2 present at 24 h (Figure 7G). Representative coronal sections from selected brain areas are provided in
3 Figure 7I, and a list of the top 15 most activated brain regions by Fc-PYY₃₋₃₆ + Fc-GLP-1 co-administration
4 is provided in Supplementary Table 1. Collectively, these data indicate that, at least in part, synergistic
5 action of Fc-PYY₃₋₃₆ + Fc-GLP-1 combination is mediated by acute activation of neuronal circuitry in the
6 CeA, PBN and NTS that is sustained up to 24 hours post-administration specifically in the NTS region of
7 the brain stem.

8

Journal Pre-proof

1 4. Discussion

2 The growing global burden of obesity and its associated comorbidities, including type 2 diabetes (T2D),
3 has necessitated development of multifaceted therapeutics that not only address glucose control and
4 weight loss, but also significantly delay the onset of comorbidities such as cardiovascular and renal
5 complications, as well as reduce the risk of several cancers [34-37]. The observation that GLP-1 and PYY₃₋₃₆
6 peptides, co-secreted from intestinal L-cells [38-40], are acutely increased after bariatric-surgery and
7 may act as effectors for reversal of type 2 diabetes independent of weight loss have led to numerous
8 investigations into the utility of GLP-1/PYY₃₋₃₆ combination therapy in obesity and diabetes [34, 35].
9 Indeed, several PYY₃₋₃₆ analogues and Y2 receptor agonists are currently being developed in combination
10 with GLP-1 analogues for this indication [33, 41, 42], and a therapeutic combination of GLP-1 and PYY₃₋₃₆
11 has demonstrated synergistic effects on energy intake in humans [11, 43, 44]. However, although clear
12 effects on energy intake and weight loss have also been observed preclinically in rodents, the
13 mechanism(s) underlying the efficacy of combining these gut-peptides has been largely unexplored [38-
14 40].

15 Here, we demonstrate impressive synergistic pharmacological effects of long-acting GLP-1 and PYY₃₋₃₆ on
16 body weight loss, glucose control, restoration of β -cell function and remission of diabetes in the
17 C57BLKS/J *db/db* mouse model of profound obesity with severe diabetes [18, 20, 45]. Moreover, in a
18 moderate model of obesity/diabetes, the DIO C57BL6/J mice, hyperinsulinemic-euglycemic clamp
19 studies revealed Fc-PYY₃₋₃₆ + Fc-GLP-1 combination treatment improved insulin sensitivity as indicated by
20 reduced insulin levels during the clamp with no significant change in hepatic glucose production yet
21 increased glucose disposal in liver, BAT and potentially skeletal muscle. The insulin sensitization could
22 not be explained by the accompanying weight loss alone. This Fc-PYY₃₋₃₆ + Fc-GLP-1 combination led to
23 activation of distinct brain regions related to appetite and energy homeostasis compared to
24 monotherapies, underlining that a coordinated central and peripheral action is likely required to be an
25 effective approach for treatment of obesity-linked T2D.

26 Considering quite inadequate β -cell adaptive compensation underlying severe type 2 diabetes in
27 C57BLKS/J *db/db* mice [18, 20, 45], the observations of normalized glycemia together with a marked
28 improvement in endogenous β -cell function with Fc-PYY₃₋₃₆ + Fc-GLP-1 combination treatment versus Fc-
29 GLP-1 monotherapy were particularly impressive. There was an apparent increase in β -cell mass as well
30 as replenishment of insulin secretory granule insulin stores paralleling an increase in total pancreatic
31 insulin content. This restoration of endogenous insulin secretory capacity in turn led to a more effective

1 biphasic glucose-stimulated insulin secretion. A cautionary note should be made about the measure of
2 β -cell mass, since insulin itself was used as a marker for this analysis. Indeed, we report a >5-fold
3 increase of insulin secretory granules with Fc-PYY₃₋₃₆ + Fc-GLP-1 treatment (Figure 2D-F), . Therefore an
4 apparent expansion of β -cell mass could actually reflect β -cell functional adaptation in restoration of
5 insulin secretory stores rather than any increase in β -cell numbers *per se* as we have previously
6 indicated [16, 18, 20, 45]. There was no direct effect of Fc-PYY₃₋₃₆ on insulin secretion *ex vivo*, thus *in vivo*
7 improvements in β -cell function by Fc-PYY₃₋₃₆ in synergy with Fc-GLP-1 are likely driven by physiological
8 alterations rather than direct action of PYY₃₋₃₆ on the β -cell itself. A consideration in these experiments is
9 the age of the animal, since our experiments were conducted in relatively young animals and may not
10 fully reflect a chronically acquired metabolic disease, like T2D. However, we did deliberately use KS
11 *db/db* mice that are β -cell deficient and not capable of sufficient compensatory β -cell mass expansion to
12 meet metabolic demand leading to earlier onset and more profound diabetes. A previous study
13 reported improved first-phase insulin secretion in overweight patients following co-administration of
14 PYY₃₋₃₆ + GLP-1, yet no additive or synergistic effect compared to GLP-1 alone [46, 47]. However, these
15 results were derived from acute exposure of these gut peptides at lower doses and not necessarily
16 comparable to the beneficial longer-term treatment using Fc-PYY₃₋₃₆ and Fc-GLP-1 which have longer
17 pharmacokinetics. Nonetheless, our data is indicative of enhanced β -cell functional recovery, that was
18 accompanied by increased expression of key genes related to normal β -cell function, in parallel to
19 improved insulin sensitivity and glucose homeostasis. Further mechanistic details of functional β -cell
20 recovery will need to be explored in future studies.

21 Preclinical rodent studies have demonstrated the weight-lowering potential of GLP-1/PYY₃₋₃₆ co-
22 administration [39], but any pharmacological effects of these combined peptides that are weight-loss
23 independent have not been elucidated. To this end, we performed experiments in C57BLKS/J *db/db*
24 mice receiving Fc-PYY₃₋₃₆ + Fc-GLP-1 combination treatment and compared to untreated, but weight-
25 matched, animals. Fc-PYY₃₋₃₆ + Fc-GLP-1 combination treatment increased 24h energy expenditure, VO₂,
26 RER and a trend towards activity relative to weight match controls and restored the more normal
27 circadian pattern of energy expenditure relative to controls during the dark phase (Figure 3c-f).
28 Interestingly total activity was reduced in the light phase relative to weight matched controls. As such,
29 some metabolic parameters influenced by Fc-PYY₃₋₃₆ + Fc-GLP-1 are independent of weight-loss.
30 However, both GLP-1 and PYY₃₋₃₆ are associated with nausea and emesis [47, 48] and consistent with
31 previous reports, we observed a taste aversive effect in monotherapy as well as combination therapy.
32 Of note, conditioned taste aversion to Fc-PYY₃₋₃₆ + Fc-GLP-1 was comparable to the chemotherapeutic

1 cisplatin, indicating aversive feeding behaviour may contribute to some of the pro-metabolic and body
2 weight loss effects Fc-PYY₃₋₃₆ + Fc-GLP-1, but the temporal relationship between dosing and the
3 pathways regulating food intake, body weight, and acute nausea remain to be clarified. As taste
4 aversion was observed with GLP-1 and PYY₃₋₃₆ monotherapies, and more so with the Fc-PYY₃₋₃₆ + Fc-GLP-
5 1 combination, in these preclinical studies at doses that correspond to significant metabolic benefit,
6 further analyses would likely be required to understand whether synergism on efficacy can be
7 uncoupled from tolerability concerns. Lower dose combinations of PYY₃₋₃₆ and GLP-1 have been
8 successful in reducing aversive effects, and dose-titration strategies to mitigate such effects of these
9 incretin class of therapeutics may be applied [33, 43, 49]. Nonetheless, the data presented here suggest
10 that substrate utilization and activity are unlikely to explain all the metabolic benefits obtained with Fc-
11 PYY₃₋₃₆ + Fc-GLP-1 combination treatment.

12 Whether improvement of glucose homeostasis is directly due to weight loss remains a fundamental
13 question in obesity treatment. Interestingly, in diabetic patients undergoing RYGB surgery, rapid
14 improvement in metabolic parameters such as blood glucose and insulin levels occur before any
15 significant weight loss is observed. This suggests that reversal of diabetes by bariatric surgery may be a
16 direct effect, rather than a secondary outcome of weight loss, that in part might be mediated by
17 increases in gut peptide hormone secretion soon after the surgery [50-52]. Here, hyperinsulinemic-
18 euglycemic clamp studies of Fc-PYY₃₋₃₆ + Fc-GLP-1-treated C57BLKS/J *db/db* mice also demonstrated
19 improved metabolic benefit compared to commensurate weight loss control animals. Insulin sensitivity
20 during the clamp was significantly improved as evidenced by a 4-fold increase in glucose-infusion rates
21 in Fc-PYY₃₋₃₆ + Fc-GLP-1 combination-treated C57BLKS/J *db/db* mice, versus weight-matched controls.
22 Both Fc-PYY₃₋₃₆ and Fc-GLP-1 agonist arms contribute to the observed metabolic efficacy of the Fc-PYY₃₋₃₆
23 + Fc-GLP-1 combination treatment as evidenced by blunted reductions in weight loss and fasting plasma
24 glucose in DIO mice lacking Y2R.

25 The weight-independent effect of Fc-PYY₃₋₃₆ + Fc-GLP-1 dual agonism in C57BLKS/J *db/db* mice on
26 glucose homeostasis, was also observed as significantly increased insulin stimulated whole-body glucose
27 disposal and suppression of hepatic glucose production relative to weight-matched controls. These
28 improvements in systemic glucose disposal could be attributed to improved insulin sensitivity, leading to
29 enhanced hepatic, BAT, and a potential degree of skeletal muscle, glucose uptake. The fate of skeletal
30 muscle glucose may have been oxidization, since insulin-stimulated glycogen synthesis did not increase.
31 Yet, insulin stimulated hepatic glycogen synthesis was strongly stimulated by Fc-PYY₃₋₃₆ + Fc-GLP-1

1 combination in C57BLKS/J *db/db* mice, over 10-fold greater than weight-matched controls, implicating a
2 more predominant mechanism for the glucose disposing effects of Fc-PYY₃₋₃₆ + Fc-GLP-1 combination
3 treatment, in line with improved hepatic insulin sensitivity. As neither Y2R nor GLP1R are expressed by
4 skeletal muscle or the liver [53, 54], the effect of Fc-PYY₃₋₃₆ + Fc-GLP-1 combination on peripheral and
5 hepatic insulin sensitization must be secondary. The absence of Y2R did not influence whole body or
6 tissue specific glucose disposal in DIO mice receiving Fc-PYY₃₋₃₆ + Fc-GLP-1 combination treatment,
7 although it did moderate liver-specific glycogen synthesis despite a clear relationship between whole
8 body glucose disposal, Y2R agonism, and plasma insulin levels during hyperinsulinemic-euglycemic
9 clamp conditions. However, these Y2RKO mouse studies were limited to much a milder and significantly
10 less insulin resistant DIO model compared to the more severely obese/diabetic C57BLKS/J *db/db* mouse
11 model.

12 Numerous studies have revealed how the brain can influence glucose homeostasis in response to
13 afferent input from peripheral signals [55-58]. The hypothalamus in particular has historically been
14 associated with regulation of both liver glycogen content and blood glucose [55]. Recent scientific
15 advances have begun to unravel the neurocircuitry involved in the regulation of blood glucose and
16 energy metabolism [59, 60], and the VMH, ARC, DMX, and PVN have all emerged as important metabolic
17 control centres of the CNS. GLP-1 is known to act through GLP-1R expressed on hypothalamic and vagal
18 sensory neurons and the central effects of endogenous brain GLP-1 are well characterized [61-63]. PYY₃₋₃₆
19 binds to NPY2R and also participates in the hypothalamic control of appetite [9, 64]. Given the
20 proposed mode of GLP-1 and PYY₃₋₃₆ dual agonistic action through the hypothalamus, hindbrain and
21 vagus nerve to regulate energy homeostasis, we speculated whether their combined pharmacology
22 might be mediated through interaction between distinct neural pathways to account for their marked
23 synergistic effect on metabolic homeostasis. An important consideration of this study is the large size of
24 the Fc molecules and their lack of ability to penetrate the blood brain barrier. Therefore the neuronal
25 signal transduction observed likely originated in the hypothalamus and or brainstem in locations that
26 lack a blood brain barrier such as the area postrema and arcuate nucleus. The Fc-PYY₃₋₃₆ + Fc-GLP-1
27 combination-treatment resulted in robust neuronal activity, as indicated by cFOS activation, in the CeA,
28 NTS, AP, BST, PBN, and PVN regions 4 h post administration. Activation of these brain regions is
29 consistent with CNS modulation of energy homeostasis [44]. While activation of the AP/NTS then to the
30 PBN and CeA regions is a plausible neuronal pathway [44], the synergistic activation by the combination
31 of GLP-1R and Y2R agonism results in a much stronger activation in the PVN and NTS regions of the

1 brain. Furthermore, gene expression analysis revealed a profound increase in the number of regulated
2 genes in the PVN versus the arcuate nucleus or nucleus of the solitary tract suggesting PVN is likely a key
3 early mediator in central activation of metabolic control. By utilizing Y2RKO models we were able to
4 further explore the role of individual receptors and found that synergistic induction of cFos activity in
5 PVN was Y2R-dependent.

6 Several brain regions showed sustained cFos expression 24 h after Fc-PYY₃₋₃₆ + Fc-GLP-1 combination-
7 treatment demonstrating persistent activity. Notably, the DMX region showed 25-fold greater
8 activation 24 h following Fc-PYY₃₋₃₆ + Fc-GLP-1 co-administration relative to vehicle. The brainstem
9 dorsal vagal complex integrates hypothalamic inputs and relays endocrine signal to peripheral organs via
10 vagal efferent fibres resulting in suppression of energy intake and hepatic glucose output [65-67]. As
11 hypothalamic and peripheral Y2R activation decreases food intake by increasing vagal afferent activity,
12 and direct activation of dorsal vagal complex by PYY₃₋₃₆ appears to increase food intake by attenuating
13 NTS and vagal afferent signalling [68], the mode of PYY₃₋₃₆ action in the brain remains unclear. Most
14 evidence points towards an inhibitory role of PYY₃₋₃₆ in NTS and vagal afferent neurons and one possible
15 mechanism of PYY-GLP-1 synergy could be through disinhibition of GLP-1 induced neuronal activity [44],
16 although has yet to be validated experimentally. Additional studies are required to characterize specific
17 neuronal populations regulated by individual receptors to better understand the mechanism underlying
18 their synergistic effect. In this regard, it should be noted that aspects of this neuronal circuitry are not
19 only involved in food intake and control of metabolic homeostasis, but also in taste aversion. As such,
20 future studies should also attempt to tease out the aversive behaviour neuronal network. If this can be
21 separated from those that control satiety and metabolic control, then non-nauseating approaches to
22 treat obesity and T2D might be pursued. Nonetheless, these results indicate that early activation of the
23 PVN and subsequent downstream stimulation of the DMX may represent an initial central activation
24 signal preceding the synergistic homeostatic improvement induced by PYY₃₋₃₆ + GLP-1 co-agonism.

25 5. Conclusions

26 In summary, a therapeutic approach using a combination of long acting Fc-PYY₃₋₃₆ + Fc-GLP-1 analogues
27 rendered profound weight loss and diabetes remission in two distinct mouse models of obesity-linked
28 T2D, reminiscent of bariatric surgery. The synergistic action of PYY₃₋₃₆ and GLP-1 was recapitulated in the
29 brain via cFOS activation in discrete regions in the hypothalamus and hindbrain which may contribute to
30 the effects on appetite control and metabolic homeostasis. These results also emphasize the current
31 concept that in alleviating insulin resistance in obesity/T2D improves glucose homeostasis to place less

1 demand on the pancreatic β -cell, and as such endogenous β -cell functional mass can be sufficiently
2 restored to benefit reversal of T2D progression.

3

4

5

6

7 **Acknowledgements**

8 The authors wish to thank the Laboratory Animal Resource staff at AstraZeneca for their assistance with
9 animal husbandry and care. We would also like to thank the Vanderbilt Mouse Metabolic Phenotyping
10 Center (MMPC) supported by NIH/NIDDK funding (DK059637).

11

12 **Author Contributions**

13 B.B.B., S.O'B., J. H.-S., A.S., D.C.H., L.L., O.P.M., J.L.T., J.S.G., and C.J.R. designed experiments; B.B.B.,
14 S.O'B., I.S., J.C.N., P.B., U.R., S.R.S., D.T., A.S., N.B., S.O., S.W., V.H., B.G., P.N., J.N., S.S., R.C.L., J.A., and
15 L.L. conducted experiments, collected, analysed and/or interpreted experimental data; B.B.B., S.S.,
16 R.C.L., D.C.H., and C.J.R. wrote the paper; B.B.B., S.S., R.C.L., O.P.M, and C.J.R. reviewed and edited the
17 manuscript.

18

19 **Financial Support:** These studies were funded by Research and Early Development, Cardiovascular,
20 Renal and Metabolism, BioPharmaceuticals R&D, AstraZeneca. The Vanderbilt Mouse Metabolic
21 Phenotyping Center (MMPC) is supported by NIH/NIDDK funding (DK059637).

22

23 **Conflicts of Interest:** BBB was previously employed by AstraZeneca PLC and Gubra ApS, and is currently
24 employed by PRECISIONscientia; JCN, PB, UR, JH-S, SRS, and DDT are currently employed by Gubra ApS;
25 PB and DDT hold shares in Gubra ApS; SB, IS, SO, SW, BG, PN, JN, SS, RCL, DCH, JSG and CJR are currently
26 employed by Astrazeneca PLC, and SB, IS, SO, SW, BG, PN, JN, RCL, DCH, JSG and CJR hold shares in the
27 company; VH is currently employed by Astrazeneca PLC and holds shares in AstraZeneca, PLC and
28 Regeneron Pharmaceuticals, LLC.; NB was previously employed by Astrazeneca PLC, is currently
29 employed by Roche and holds shares in Roche; AS was previously employed by Astrazeneca PLC and
30 hold shares in DTXPharma. JLT was previously employed by Astrazeneca PLC, is currently employed by
31 Gilead Sciences, Inc. and holds shares in Gilead Sciences, Inc.

1
2
3
4
5
6
7
8
9
10
11
12
13
14
15
16
17
18
19
20
21
22
23
24
25
26
27
28
29
30
31
32
33
34
35
36
37
38
39
40
41
42
43
44
45

References

- [1] K. M. Gadde, C. K. Martin, H. R. Berthoud, and S. B. Heymsfield, "Obesity: Pathophysiology and Management," *J Am Coll Cardiol*, vol. 71, no. 1, pp. 69-84, Jan 2 2018.
- [2] J. L. Kraschnewski *et al.*, "Long-term weight loss maintenance in the United States," *Int J Obes (Lond)*, vol. 34, no. 11, pp. 1644-54, Nov 2010.
- [3] L. R. Madsen, L. M. Baggesen, B. Richelsen, and R. W. Thomsen, "Effect of Roux-en-Y gastric bypass surgery on diabetes remission and complications in individuals with type 2 diabetes: a Danish population-based matched cohort study," *Diabetologia*, vol. 62, no. 4, pp. 611-620, Apr 2019.
- [4] L. Sjostrom, "Review of the key results from the Swedish Obese Subjects (SOS) trial - a prospective controlled intervention study of bariatric surgery," *J Intern Med*, vol. 273, no. 3, pp. 219-34, Mar 2013.
- [5] C. W. le Roux *et al.*, "Gut hormones as mediators of appetite and weight loss after Roux-en-Y gastric bypass," *Ann Surg*, vol. 246, no. 5, pp. 780-5, Nov 2007.
- [6] D. J. Drucker, "Mechanisms of Action and Therapeutic Application of Glucagon-like Peptide-1," *Cell Metab*, vol. 27, no. 4, pp. 740-756, Apr 3 2018.
- [7] S. Sisley, R. Gutierrez-Aguilar, M. Scott, D. A. D'Alessio, D. A. Sandoval, and R. J. Seeley, "Neuronal GLP1R mediates liraglutide's anorectic but not glucose-lowering effect," *J Clin Invest*, vol. 124, no. 6, pp. 2456-63, Jun 2014.
- [8] E. M. Varin *et al.*, "Distinct Neural Sites of GLP-1R Expression Mediate Physiological versus Pharmacological Control of Incretin Action," *Cell Rep*, vol. 27, no. 11, pp. 3371-3384 e3, Jun 11 2019.
- [9] R. L. Batterham *et al.*, "Gut hormone PYY(3-36) physiologically inhibits food intake," *Nature*, vol. 418, no. 6898, pp. 650-4, Aug 8 2002.
- [10] C. R. Abbott *et al.*, "The inhibitory effects of peripheral administration of peptide YY(3-36) and glucagon-like peptide-1 on food intake are attenuated by ablation of the vagal-brainstem-hypothalamic pathway," *Brain Res*, vol. 1044, no. 1, pp. 127-31, May 17 2005.
- [11] J. B. Schmidt *et al.*, "Effects of PYY3-36 and GLP-1 on energy intake, energy expenditure, and appetite in overweight men," *Am J Physiol Endocrinol Metab*, vol. 306, no. 11, pp. E1248-56, Jun 1 2014.
- [12] J. Sambrook and D. Russell, *Molecular Cloning: A Laboratory Manual (3-Volume Set)*. 2001.
- [13] R. Butler *et al.*, "Use of the site-specific retargeting jump-in platform cell line to support biologic drug discovery," *J Biomol Screen*, vol. 20, no. 4, pp. 528-35, Apr 2015.
- [14] J. Naylor, A. Rossi, and D. C. Hornigold, "Acoustic Dispensing Preserves the Potency of Therapeutic Peptides throughout the Entire Drug Discovery Workflow," (in eng), no. 2211-0690 (Electronic).
- [15] B. Boland *et al.*, "The PYY/Y2R-Deficient Mouse Responds Normally to High-Fat Diet and Gastric Bypass Surgery," *Nutrients*, vol. 11, no. 3, Mar 10 2019.
- [16] B. B. Boland *et al.*, "Combined loss of GLP-1R and Y2R does not alter progression of high-fat diet-induced obesity or response to RYGB surgery in mice," *Mol Metab*, vol. 25, pp. 64-72, Jul 2019.
- [17] B. B. Boland, C. Brown, Jr., C. Alarcon, D. Demozay, J. S. Grimsby, and C. J. Rhodes, "beta-Cell Control of Insulin Production During Starvation-Refeeding in Male Rats," *Endocrinology*, vol. 159, no. 2, pp. 895-906, Feb 1 2018.

- 1 [18] B. B. Boland *et al.*, "Pancreatic beta-Cell Rest Replenishes Insulin Secretory Capacity and
2 Attenuates Diabetes in an Extreme Model of Obese Type 2 Diabetes," *Diabetes*, vol. 68, no. 1,
3 pp. 131-140, Jan 2019.
- 4 [19] K. Yaekura *et al.*, "Insulin secretory deficiency and glucose intolerance in Rab3A null mice," *J Biol*
5 *Chem*, vol. 278, no. 11, pp. 9715-21, Mar 14 2003.
- 6 [20] C. Alarcon *et al.*, "Pancreatic beta-Cell Adaptive Plasticity in Obesity Increases Insulin Production
7 but Adversely Affects Secretory Function," *Diabetes*, vol. 65, no. 2, pp. 438-50, Feb 2016.
- 8 [21] M. L. Boland *et al.*, "Resolution of NASH and hepatic fibrosis by the GLP-1R/GcgR dual-agonist
9 Cotadutide via modulating mitochondrial function and lipogenesis," *Nat Metab*, vol. 2, no. 5, pp.
10 413-431, May 2020.
- 11 [22] T. M. Chan and J. H. Exton, "A rapid method for the determination of glycogen content and
12 radioactivity in small quantities of tissue or isolated hepatocytes," *Anal Biochem*, vol. 71, no. 1,
13 pp. 96-105, Mar 1976.
- 14 [23] J. Jelsing, A. M. Galzin, E. Guillot, M. P. Pruniaux, P. J. Larsen, and N. Vrang, "Localization and
15 phenotypic characterization of brainstem neurons activated by rimonabant and WIN55,212-2,"
16 *Brain Res Bull*, vol. 78, no. 4-5, pp. 202-10, Mar 16 2009.
- 17 [24] C. Zhang *et al.*, "The dorsomedial hypothalamus and nucleus of the solitary tract as key
18 regulators in a rat model of chronic obesity," *Brain Res*, vol. 1727, p. 146538, Jan 15 2020.
- 19 [25] R. Edgar, M. Domrachev, and A. E. Lash, "Gene Expression Omnibus: NCBI gene expression and
20 hybridization array data repository," *Nucleic Acids Res*, vol. 30, no. 1, pp. 207-10, Jan 1 2002.
- 21 [26] A. Dobin *et al.*, "STAR: ultrafast universal RNA-seq aligner," *Bioinformatics*, vol. 29, no. 1, pp. 15-
22 21, Jan 1 2013.
- 23 [27] M. I. Love, W. Huber, and S. Anders, "Moderated estimation of fold change and dispersion for
24 RNA-seq data with DESeq2," *Genome Biol*, vol. 15, no. 12, p. 550, 2014.
- 25 [28] L. Varemò, J. Nielsen, and I. Nookaew, "Enriching the gene set analysis of genome-wide data by
26 incorporating directionality of gene expression and combining statistical hypotheses and
27 methods," *Nucleic Acids Res*, vol. 41, no. 8, pp. 4378-91, Apr 2013.
- 28 [29] R. Haw and L. Stein, "Using the reactome database," *Curr Protoc Bioinformatics*, vol. Chapter 8,
29 p. Unit8 7, Jun 2012.
- 30 [30] N. Renier, Z. Wu, D. J. Simon, J. Yang, P. Ariel, and M. Tessier-Lavigne, "iDISCO: a simple, rapid
31 method to immunolabel large tissue samples for volume imaging," *Cell*, vol. 159, no. 4, pp. 896-
32 910, Nov 6 2014.
- 33 [31] S. W. Oh *et al.*, "A mesoscale connectome of the mouse brain," *Nature*, vol. 508, no. 7495, pp.
34 207-14, Apr 10 2014.
- 35 [32] A. I. Mina, R. A. LeClair, K. B. LeClair, D. E. Cohen, L. Lantier, and A. S. Banks, "CalR: A Web-Based
36 Analysis Tool for Indirect Calorimetry Experiments," *Cell Metab*, vol. 28, no. 4, pp. 656-666 e1,
37 Oct 2 2018.
- 38 [33] S. M. Rangwala *et al.*, "A Long-Acting PYY3-36 Analog Mediates Robust Anorectic Efficacy with
39 Minimal Emesis in Nonhuman Primates," *Cell Metab*, vol. 29, no. 4, pp. 837-843 e5, Apr 2 2019.
- 40 [34] R. D. Ramracheya *et al.*, "PYY-Dependent Restoration of Impaired Insulin and Glucagon
41 Secretion in Type 2 Diabetes following Roux-En-Y Gastric Bypass Surgery," *Cell Rep*, vol. 15, no.
42 5, pp. 944-950, May 3 2016.
- 43 [35] C. Guida *et al.*, "PYY plays a key role in the resolution of diabetes following bariatric surgery in
44 humans," *EBioMedicine*, vol. 40, pp. 67-76, Feb 2019.
- 45 [36] D. F. Quail and A. J. Dannenberg, "The obese adipose tissue microenvironment in cancer
46 development and progression," *Nat Rev Endocrinol*, vol. 15, no. 3, pp. 139-154, Mar 2019.
- 47 [37] J. E. Hall, J. M. do Carmo, A. A. da Silva, Z. Wang, and M. E. Hall, "Obesity, kidney dysfunction
48 and hypertension: mechanistic links," *Nat Rev Nephrol*, vol. 15, no. 6, pp. 367-385, Jun 2019.

- 1 [38] T. Talsania, Y. Anini, S. Siu, D. J. Drucker, and P. L. Brubaker, "Peripheral exendin-4 and peptide
2 YY(3-36) synergistically reduce food intake through different mechanisms in mice,"
3 *Endocrinology*, vol. 146, no. 9, pp. 3748-56, Sep 2005.
- 4 [39] L. S. Dalboge *et al.*, "A Hamster Model of Diet-Induced Obesity for Preclinical Evaluation of Anti-
5 Obesity, Anti-Diabetic and Lipid Modulating Agents," *PLoS One*, vol. 10, no. 8, p. e0135634,
6 2015.
- 7 [40] A. M. Habib, P. Richards, G. J. Rogers, F. Reimann, and F. M. Gribble, "Co-localisation and
8 secretion of glucagon-like peptide 1 and peptide YY from primary cultured human L cells,"
9 *Diabetologia*, vol. 56, no. 6, pp. 1413-6, Jun 2013.
- 10 [41] O. G. Chepurny *et al.*, "Chimeric peptide EP45 as a dual agonist at GLP-1 and NPY2R receptors,"
11 *Sci Rep*, vol. 8, no. 1, p. 3749, Feb 28 2018.
- 12 [42] B. C. Field *et al.*, "PYY3-36 and oxyntomodulin can be additive in their effect on food intake in
13 overweight and obese humans," *Diabetes*, vol. 59, no. 7, pp. 1635-9, Jul 2010.
- 14 [43] A. De Silva *et al.*, "The gut hormones PYY 3-36 and GLP-1 7-36 amide reduce food intake and
15 modulate brain activity in appetite centers in humans," *Cell Metab*, vol. 14, no. 5, pp. 700-6, Nov
16 2 2011.
- 17 [44] M. Kjaergaard, C. B. G. Salinas, J. F. Rehfeld, A. Secher, K. Raun, and B. S. Wulff, "PYY(3-36) and
18 exendin-4 reduce food intake and activate neuronal circuits in a synergistic manner in mice,"
19 *Neuropeptides*, vol. 73, pp. 89-95, Feb 2019.
- 20 [45] R. Puff *et al.*, "Reduced proliferation and a high apoptotic frequency of pancreatic beta cells
21 contribute to genetically-determined diabetes susceptibility of db/db BKS mice," *Horm Metab
22 Res*, vol. 43, no. 5, pp. 306-11, May 2011.
- 23 [46] T. M. Tan *et al.*, "Combination of peptide YY3-36 with GLP-1(7-36) amide causes an increase in
24 first-phase insulin secretion after IV glucose," *J Clin Endocrinol Metab*, vol. 99, no. 11, pp. E2317-
25 24, Nov 2014.
- 26 [47] L. Degen *et al.*, "Effect of peptide YY3-36 on food intake in humans," *Gastroenterology*, vol. 129,
27 no. 5, pp. 1430-6, Nov 2005.
- 28 [48] K. Bettge, M. Kahle, M. S. Abd El Aziz, J. J. Meier, and M. A. Nauck, "Occurrence of nausea,
29 vomiting and diarrhoea reported as adverse events in clinical trials studying glucagon-like
30 peptide-1 receptor agonists: A systematic analysis of published clinical trials," *Diabetes Obes
31 Metab*, vol. 19, no. 3, pp. 336-347, Mar 2017.
- 32 [49] N. M. Neary *et al.*, "Peptide YY3-36 and glucagon-like peptide-17-36 inhibit food intake
33 additively," *Endocrinology*, vol. 146, no. 12, pp. 5120-7, Dec 2005.
- 34 [50] C. Dirksen *et al.*, "Exaggerated release and preserved insulinotropic action of glucagon-like
35 peptide-1 underlie insulin hypersecretion in glucose-tolerant individuals after Roux-en-Y gastric
36 bypass," *Diabetologia*, vol. 56, no. 12, pp. 2679-87, Dec 2013.
- 37 [51] C. Guidone *et al.*, "Mechanisms of recovery from type 2 diabetes after malabsorptive bariatric
38 surgery," *Diabetes*, vol. 55, no. 7, pp. 2025-31, Jul 2006.
- 39 [52] C. Martinussen *et al.*, "Immediate enhancement of first-phase insulin secretion and unchanged
40 glucose effectiveness in patients with type 2 diabetes after Roux-en-Y gastric bypass," *Am J
41 Physiol Endocrinol Metab*, vol. 308, no. 6, pp. E535-44, Mar 15 2015.
- 42 [53] W. Dai *et al.*, "Expression of neuropeptide Y is increased in an activated human HSC cell line," *Sci
43 Rep*, vol. 9, no. 1, p. 9500, Jul 1 2019.
- 44 [54] N. Panjwani *et al.*, "GLP-1 receptor activation indirectly reduces hepatic lipid accumulation but
45 does not attenuate development of atherosclerosis in diabetic male ApoE(-/-) mice,"
46 *Endocrinology*, vol. 154, no. 1, pp. 127-39, Jan 2013.
- 47 [55] T. Shimazu, "Innervation of the liver and gluco-regulation: roles of the hypothalamus and
48 autonomic nerves," *Nutrition*, vol. 12, no. 1, pp. 65-6, Jan 1996.

- 1 [56] M. A. Bentsen, Z. Mirzadeh, and M. W. Schwartz, "Revisiting How the Brain Senses Glucose-And
2 Why," *Cell Metab*, vol. 29, no. 1, pp. 11-17, Jan 8 2019.
- 3 [57] M. G. Myers, Jr. and D. P. Olson, "Central nervous system control of metabolism," *Nature*, vol.
4 491, no. 7424, pp. 357-63, Nov 15 2012.
- 5 [58] J. Ruud, S. M. Steculorum, and J. C. Bruning, "Neuronal control of peripheral insulin sensitivity
6 and glucose metabolism," *Nat Commun*, vol. 8, p. 15259, May 4 2017.
- 7 [59] T. Klockener *et al.*, "High-fat feeding promotes obesity via insulin receptor/PI3K-dependent
8 inhibition of SF-1 VMH neurons," *Nat Neurosci*, vol. 14, no. 7, pp. 911-8, Jun 5 2011.
- 9 [60] T. H. Meek *et al.*, "Functional identification of a neurocircuit regulating blood glucose," *Proc Natl
10 Acad Sci U S A*, vol. 113, no. 14, pp. E2073-82, Apr 5 2016.
- 11 [61] L. Lopez-Ferreras *et al.*, "Lateral hypothalamic GLP-1 receptors are critical for the control of food
12 reinforcement, ingestive behavior and body weight," *Mol Psychiatry*, vol. 23, no. 5, pp. 1157-
13 1168, May 2018.
- 14 [62] S. E. Kanoski, S. M. Fortin, M. Arnold, H. J. Grill, and M. R. Hayes, "Peripheral and central GLP-1
15 receptor populations mediate the anorectic effects of peripherally administered GLP-1 receptor
16 agonists, liraglutide and exendin-4," *Endocrinology*, vol. 152, no. 8, pp. 3103-12, Aug 2011.
- 17 [63] T. P. Vahl *et al.*, "Glucagon-like peptide-1 (GLP-1) receptors expressed on nerve terminals in the
18 portal vein mediate the effects of endogenous GLP-1 on glucose tolerance in rats,"
19 *Endocrinology*, vol. 148, no. 10, pp. 4965-73, Oct 2007.
- 20 [64] C. Broberger, M. Landry, H. Wong, J. N. Walsh, and T. Hokfelt, "Subtypes Y1 and Y2 of the
21 neuropeptide Y receptor are respectively expressed in pro-opiomelanocortin- and
22 neuropeptide-Y-containing neurons of the rat hypothalamic arcuate nucleus,"
23 *Neuroendocrinology*, vol. 66, no. 6, pp. 393-408, Dec 1997.
- 24 [65] H. J. Grill and M. R. Hayes, "Hindbrain neurons as an essential hub in the neuroanatomically
25 distributed control of energy balance," *Cell Metab*, vol. 16, no. 3, pp. 296-309, Sep 5 2012.
- 26 [66] C. K. Lam, M. Chari, G. A. Rutter, and T. K. Lam, "Hypothalamic nutrient sensing activates a
27 forebrain-hindbrain neuronal circuit to regulate glucose production in vivo," *Diabetes*, vol. 60,
28 no. 1, pp. 107-13, Jan 2011.
- 29 [67] J. Rossi *et al.*, "Melanocortin-4 receptors expressed by cholinergic neurons regulate energy
30 balance and glucose homeostasis," *Cell Metab*, vol. 13, no. 2, pp. 195-204, Feb 2 2011.
- 31 [68] N. J. Huston, L. A. Brenner, Z. C. Taylor, and R. C. Ritter, "NPY2 receptor activation in the dorsal
32 vagal complex increases food intake and attenuates CCK-induced satiation in male rats," *Am J
33 Physiol Regul Integr Comp Physiol*, vol. 316, no. 4, pp. R406-R416, Apr 1 2019.
- 34
- 35

1 **Figure Legends**

2 **Figure 1: Physiological parameters of male KS *db/db* mice administered Fc-PYY₃₋₃₆ (1 mg/kg),**
 3 **Fc-GLP-1 agonist (0.15 mg/kg) or Fc-PYY₃₋₃₆/GLP-1 agonist combination (1 mg/kg/0.15 mg/kg).**
 4 A) Body weight profile of 8-week old animals during the 4-week treatment period. B) Change in
 5 body mass following 4 weeks of treatment. N=20 for all groups. C) Change in %hbA1c following
 6 4 weeks of treatment. N=8 for all groups D) 6-hour fasted ipGTT (2g/kg) and E) associated AUC
 7 after 3 weeks of treatment. F) Fasting plasma glucose and G) fasting plasma insulin following 3
 8 weeks of treatment. N=12 for all groups. H) Pancreatic insulin content at study termination.
 9 N=4 for all groups. * $p \leq 0.05$ vs Vehicle, ** $p \leq 0.01$ vs Vehicle, *** $p \leq 0.001$ vs Vehicle, **** $p \leq$
 10 0.0001 vs Vehicle.

11 **Figure 2: Effect of 4 week Fc-PYY₃₋₃₆/GLP-1 (1 mg/kg/0.15 mg/kg) combination treatment on**
 12 **β -cell function in KS *db/db* mice.** A) Perifusion of freshly isolated islets and B) 1st and 2nd phase
 13 perifusion AUC. N=4-5. C) Freshly isolated islet RT-qPCR for *Ins1*, *Ins2*, *Gck*, *Slca2a*, *Pdx1*, and
 14 *Mafa*. *Rnas18s* used as housekeeping. Data presented as relative expression versus vehicle.
 15 N=5-6. D) Representative transmission electron micrograph of islets isolated from Vehicle and E)
 16 combination-treated animals. F) Quantification of mature insulin granule area and G) immature
 17 insulin granule area per total cytoplasmic area. N=3-4 from >10 representative electron
 18 micrographs. H) β/α -cell mass from insulin/glucagon dual-stained immunohistochemistry
 19 sections. N=3-4. I) Effect of Fc-PYY₃₋₃₆, Fc-GLP-1, and the combination on overnight cultured
 20 C57BL/6J islet insulin secretion and the J) associated insulin AUC. N \geq 3. *** $p \leq 0.001$ vs Vehicle,
 21 **** $p \leq 0.0001$ vs Vehicle.

22 **Figure 3: Effect of 2 week Fc-PYY₃₋₃₆/GLP-1 (1 mg/kg/0.15 mg/kg) treatment on energy**
 23 **expenditure in KS *db/db* mice.** A) Body weight profile of study animals and B) the percent
 24 change in body weight during the 2-week treatment period. N=8 for all groups. Dashed line
 25 indicates beginning of acclimation to indirect calorimetry cages. Indirect calorimetry recording
 26 began on day 14. * $p \leq 0.05$ *db/db* vs *db/db* Fc-PYY₃₋₃₆/GLP-1, # $p \leq 0.05$ *db/db* vs *db/db* WM. C)
 27 real-time vO_2 and D) vO_2 from 48-hr light (24 hr) and dark (24 hr) periods. E) RER, F) regression
 28 plot of energy expenditure as a function of body weight and G) total activity from 48-hr light (24
 29 hr) and dark (24 hr) periods. N=8 for all groups. ** $p \leq 0.01$ vs Vehicle, *** $p \leq 0.001$ vs Vehicle,
 30 **** $p \leq 0.0001$ vs Vehicle. Asterisks above a line indicate significance between groups.

31 **Figure 4: Hyperinsulinemic/euglycemic clamp following 2 week Fc-PYY₃₋₃₆/GLP-1 (1**
 32 **mg/kg/0.15 mg/kg) treatment in KS *db/db* mice.** A) Body weight profile of study animals. B)
 33 Plasma glucose levels during the clamp. C) Glucose infusion rate required to maintain
 34 euglycemia (200 mg/dL) during the clamp. * $p \leq 0.05$ *db/db* vs *db/db* Fc-PYY₃₋₃₆/GLP-1, # $p \leq 0.05$
 35 *db/db* vs *db/db* WM. D) Basal and insulin-stimulated plasma insulin levels. E) Basal and insulin-
 36 stimulated peripheral glucose disposal (Rd). F) Basal and insulin-stimulated endogenous glucose
 37 production (Rg). G) Tissue-specific insulin-stimulated glucose disposal for gastrocnemius, vastus
 38 lateralis, soleus, perigonadal and subcutaneous adipose tissue and H) heart, brown adipose
 39 tissue and brain. I) Core liver glycogen. J) Direct liver glycogen synthesis. K) Core muscle
 40 glycogen. L) Direct muscle glycogen synthesis. N=5-10. # $p \leq 0.05$, ## $p \leq 0.01$, ### $p \leq 0.001$,

1 ##### $p \leq 0.0001$ vs $db/+$. * $p \leq 0.05$, ** $p \leq 0.01$, *** $p \leq 0.001$, **** $p \leq 0.0001$ vs db/db vehicle.
 2 $\wedge p \leq 0.05$, $\wedge\wedge p \leq 0.01$, $\wedge\wedge\wedge p \leq 0.001$, $\wedge\wedge\wedge\wedge p \leq 0.0001$, Fc-PYY₃₋₃₆/GLP-1 vs WM. For (A-C) Sidak's
 3 multiple comparisons test $db/+$ vs db/db to determine effect of genotype. One-way ANOVA
 4 with repeated measured followed by Tukey's multiple comparisons test with $db/+$ excluded to
 5 determine effect of treatment. For (D-L) unpaired t-test $db/+$ vs db/db to determine effect of
 6 genotype. One-way ANOVA followed by Tukey's multiple comparisons test with $db/+$ excluded
 7 to determine effect of treatment.

8 **Figure 5: Hyperinsulinemic/euglycemic clamp following 2 week Fc-PYY₃₋₃₆/GLP-1 (1**
 9 **mg/kg/0.15 mg/kg) treatment in DIO WT and Y2RKO mice.** A) Body weight profile of study
 10 animals. B) Plasma glucose levels during the clamp. C) Glucose infusion rate required to
 11 maintain euglycemia (110 mg/dL) during the clamp. * $p \leq 0.05$ WT Vehicle vs WT Fc-PYY₃₋₃₆/GLP-
 12 1, # $p \leq 0.05$ WT Vehicle vs Y2RKO Fc-PYY₃₋₃₆/GLP-1. D) Basal and insulin-stimulated plasma
 13 insulin levels. E) Basal and insulin-stimulated peripheral glucose disposal (Rd). F) Basal and
 14 insulin-stimulated endogenous glucose production (Rg). G) Tissue-specific insulin-stimulated
 15 glucose disposal for gastrocnemius, vastus lateralis, soleus, perigonadal and subcutaneous
 16 adipose tissue and H) heart, brown adipose tissue and brain. I) Core liver glycogen. J) Direct
 17 liver glycogen synthesis. K) Core muscle glycogen. L) Direct muscle glycogen synthesis. N=5-10.
 18 * $p \leq 0.05$, ** $p \leq 0.01$, *** $p \leq 0.001$, **** $p \leq 0.0001$, vs vehicle within genotype. # $p \leq 0.05$, ## p
 19 ≤ 0.01 , #### $p \leq 0.0001$ WT vs Y2RKO within treatment. For (A-C) two-way ANOVA with
 20 repeated measures followed by Tukey's multiple comparisons test. For (D-L) two-way ANOVA
 21 followed by Sidak's multiple comparisons test.

22 **Figure 6: Quantitation of cFOS-positive cells in selected brain regions of lean WT, Y2RKO, and**
 23 **Y2RKO/GLP1RKO mice 4 hours following IP-administered Fc-PYY₃₋₃₆ (1.0 mg/kg), Fc-GLP-1**
 24 **(0.15 mg/kg) or Fc-PYY₃₋₃₆/GLP-1 (1.0 mg/kg / 0.15 mg/kg) combination.** The average stained
 25 number of cFOS positive cells in the A) central nucleus of the amygdala (CeA), B) arcuate
 26 nucleus (ARC), C) ventromedial hypothalamic nucleus (VMH), D) bed of the stria terminalis
 27 (BST), E) parabrachial nucleus (PBN), F) area postrema (AP), G) nucleus of the solitary tract
 28 (NTS), and H) paraventricular hypothalamic nucleus (PVN) are shown. * $p \leq 0.05$ vs Vehicle,
 29 same genotype # $p \leq$ vs WT, same treatment. N=2-5.

30 **Figure 7: Whole brain cFOS quantitation of selected brain regions 24 hours following IP-**
 31 **administered Fc-PYY₃₋₃₆ (1.0 mg/kg), Fc-GLP-1 (0.5 mg/kg) or Fc-PYY₃₋₃₆/GLP-1 (1.0 mg/kg / 0.5**
 32 **mg/kg) combination in lean C57BL6J mice.** Total number of cFOS positive cells in the A)
 33 arcuate nucleus (ARC), B) paraventricular nucleus (PVN), C) area postrema (AP), D) bed of the
 34 stria terminalis (BST), E) central nucleus of the amygdala (CeA), F) parabrachial nucleus (PBN),
 35 G) nucleus of the solitary tract (NTS), H) dorsal motor nucleus of the vagal nerve (DMX) as
 36 assessed by light sheet fluorescent microscopy. I) Selected coronal sections from group
 37 averaged brains (scale bar = 1 mm). Brain regions delineated by dashed outline.

Figure 1

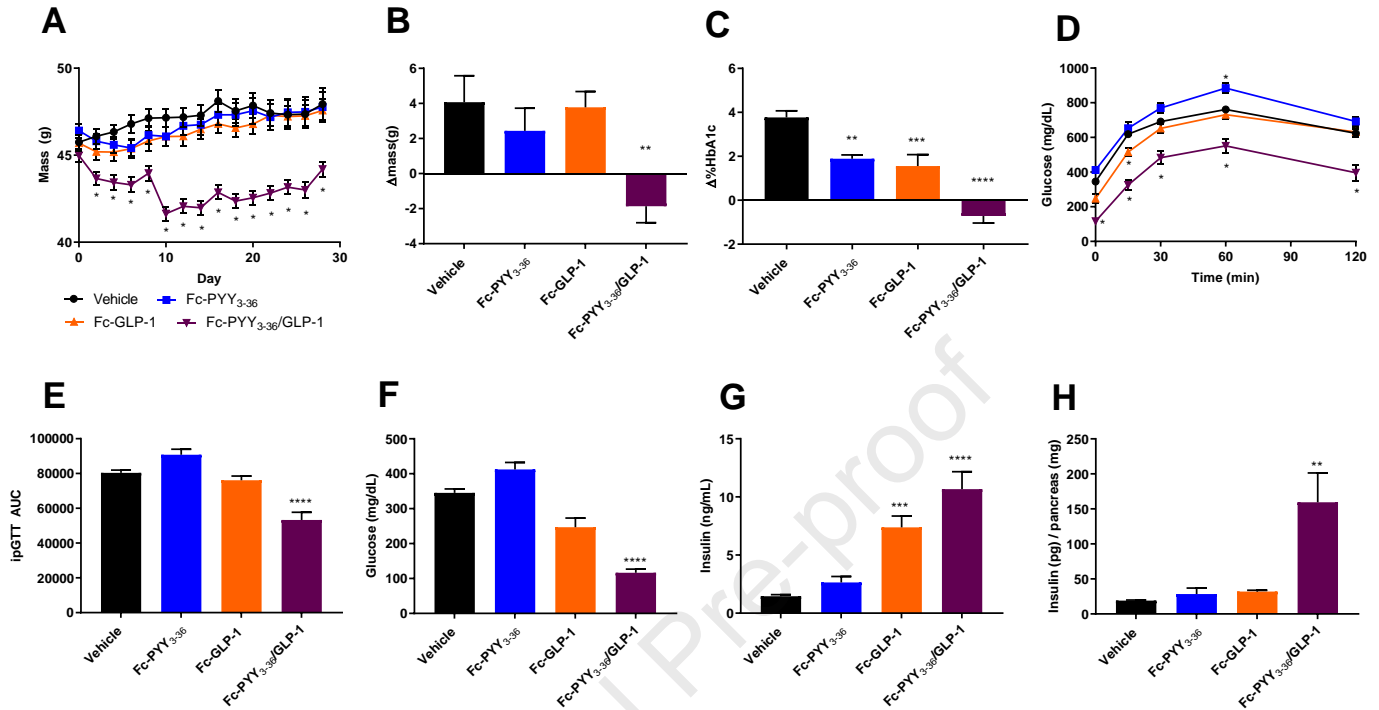


Figure 1: Physiological parameters of male KS *db/db* mice administered Fc-PYY₃₋₃₆ (1 mg/kg), Fc-GLP-1 agonist (0.15 mg/kg) or Fc-PYY₃₋₃₆/GLP-1 agonist combination (1 mg/kg/0.15 mg/kg). A) Body weight profile of 8-week old animals during the 4-week treatment period. B) Change in body mass following 4 weeks of treatment. N=20 for all groups. C) Change in %HbA1c following 4 weeks of treatment. N=8 for all groups. D) 6-hour fasted ipGTT (2g/kg) and E) associated AUC after 3 weeks of treatment. F) Fasting plasma glucose and G) fasting plasma insulin following 3 weeks of treatment. N=12 for all groups. H) Pancreatic insulin content at study termination. N=4 for all groups. * $p \leq 0.05$ vs Vehicle, ** $p \leq 0.01$ vs Vehicle, *** $p \leq 0.001$ vs Vehicle, **** $p \leq 0.0001$ vs Vehicle.

Figure 2

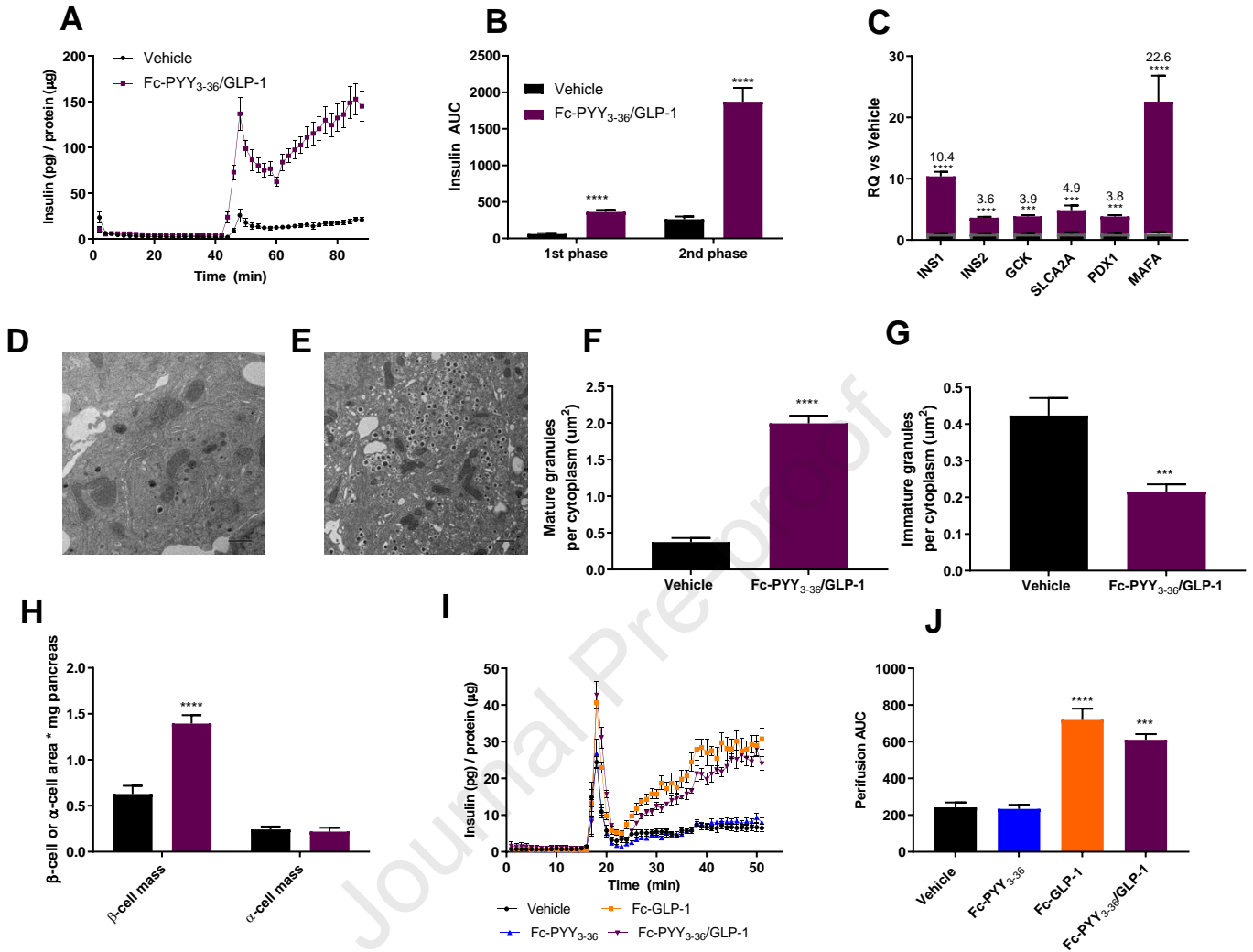


Figure 2: Effect of 4 week Fc-PYY₃₋₃₆/GLP-1 (1 mg/kg/0.15 mg/kg) combination treatment on β-cell function in KS *db/db* mice. A) Perfusion of freshly isolated islets and B) 1st and 2nd phase perfusion AUC. N=4-5. C) Freshly isolated islet RT-qPCR for *Ins1*, *Ins2*, *Gck*, *Slca2a*, *Pdx1*, and *Mafa*. *Rnas18s* used as housekeeping. Data presented as relative expression versus vehicle. N=5-6. D) Representative scanning electron micrograph of islets isolated from Vehicle and E) combination-treated animals. F) Quantification of mature insulin granule area and G) immature insulin granule area per total cytoplasmic area. N=3-4 from >10 representative electron micrographs. H) β/α-cell mass from insulin/glucagon dual-stained immunohistochemistry sections. N=3-4. I) Effect of Fc-PYY₃₋₃₆, Fc-GLP-1, and the combination on overnight cultured C57BL/6J islet insulin secretion and the J) associated insulin AUC. N≥3. ****p* ≤ 0.001 vs Vehicle, *****p* ≤ 0.0001 vs Vehicle.

Figure 3

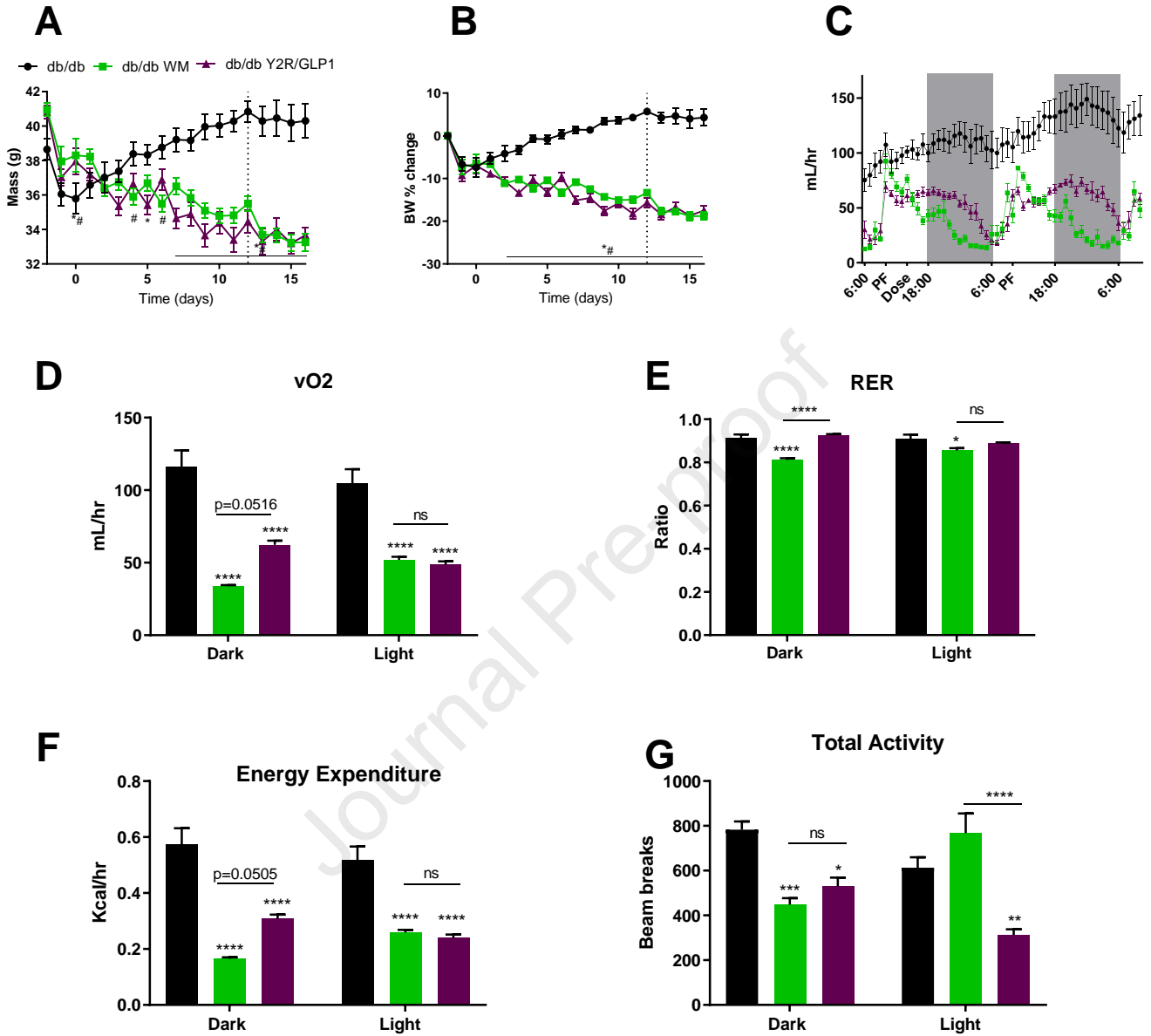


Figure 3: Effect of 2 week Fc-PYY₃₋₃₆/GLP-1 (1 mg/kg/0.15 mg/kg) treatment on energy expenditure in KS *db/db* mice. A) Body weight profile of study animals and B) the percent change in body weight during the 2-week treatment period. N=8 for all groups. Dashed line indicates beginning of acclimation to indirect calorimetry cages. Indirect calorimetry recording began on day 14. * $p \leq 0.05$ *db/db* vs *db/db* Fc-PYY₃₋₃₆/GLP-1, # $p \leq 0.05$ *db/db* vs *db/db* WM. C) real-time vO₂ and D) vO₂ from 48-hr light (24 hr) and dark (24 hr) periods. E) RER, F) energy expenditure and G) total activity from 48-hr light (24 hr) and dark (24 hr) periods. N=8 for all groups. ** $p \leq 0.01$ vs Vehicle, *** $p \leq 0.001$ vs Vehicle, **** $p \leq 0.0001$ vs Vehicle. Asterisks above a line indicate significance between groups.

Figure 4

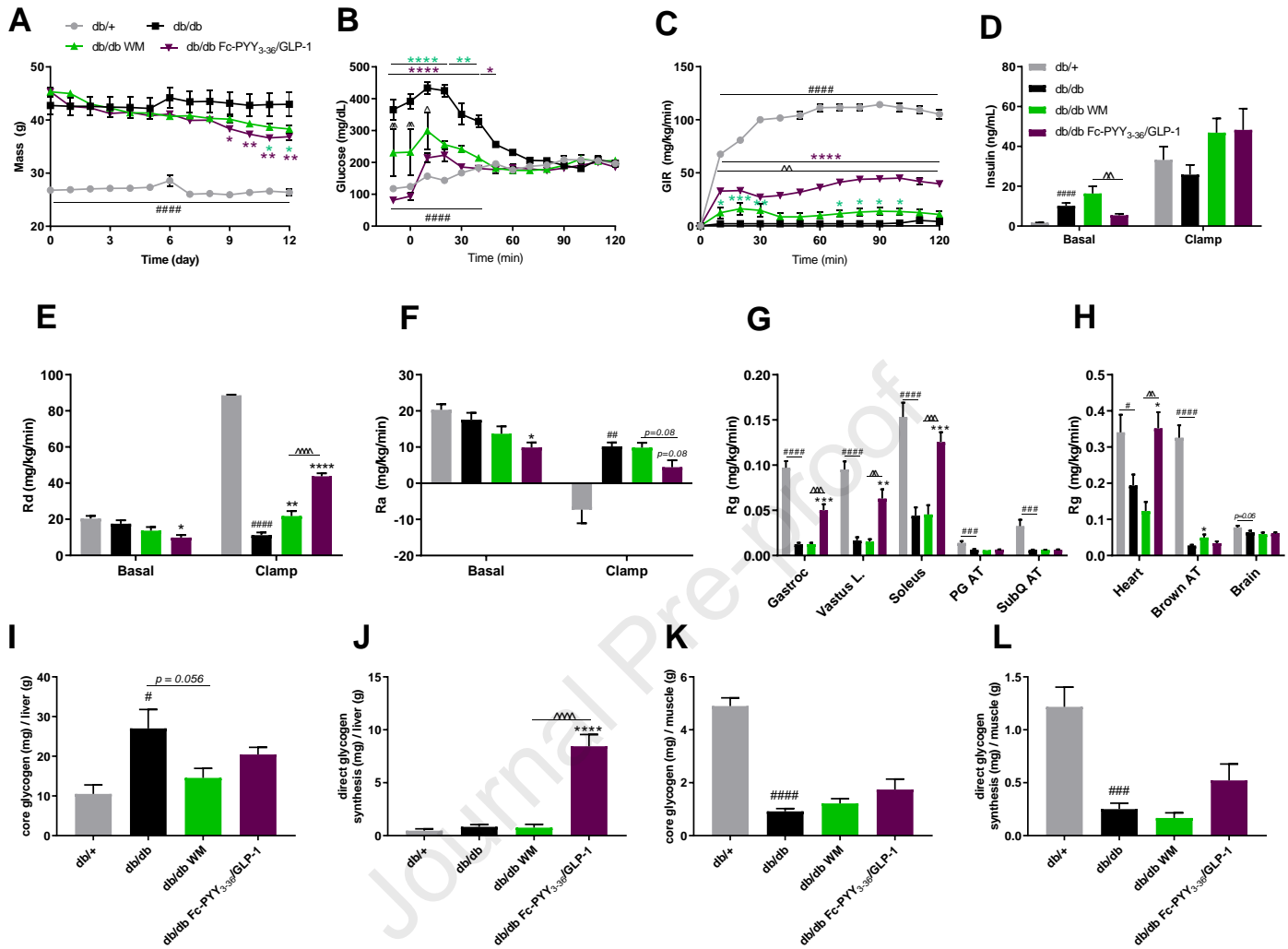


Figure 4: Hyperinsulinemic/euglycemic clamp following 2 week Fc-PYY₃₋₃₆/GLP-1 (1 mg/kg/0.15 mg/kg) treatment in KS db/db mice. A) Body weight profile of study animals. B) Plasma glucose levels during the clamp. C) Glucose infusion rate required to maintain euglycemia (200 mg/dL) during the clamp. * $p \leq 0.05$ db/db vs db/db Fc-PYY₃₋₃₆/GLP-1, # $p \leq 0.05$ db/db vs db/db WM. D) Basal and insulin-stimulated plasma insulin levels. E) Basal and insulin-stimulated peripheral glucose disposal (Rd). F) Basal and insulin-stimulated endogenous glucose production (Rg). G) Tissue-specific insulin-stimulated glucose disposal for gastrocnemius, vastus lateralis, soleus, perigonadal and subcutaneous adipose tissue and H) heart, brown adipose tissue and brain. I) Core liver glycogen. J) Direct liver glycogen synthesis. K) Core muscle glycogen. L) Direct muscle glycogen synthesis. N=5-10. # $p \leq 0.05$, ### $p \leq 0.01$, #### $p \leq 0.001$, ##### $p \leq 0.0001$ vs $db/+$. * $p \leq 0.05$, ** $p \leq 0.01$, *** $p \leq 0.001$, **** $p \leq 0.0001$ vs db/db vehicle. ^ $p \leq 0.05$, ^^ $p \leq 0.01$, ^^ $p \leq 0.001$, ^^ $p \leq 0.0001$, Fc-PYY₃₋₃₆/GLP-1 vs WM. For (A-C) Sidak's multiple comparisons test $db/+$ vs db/db to determine effect of genotype. One-way ANOVA with repeated measured followed by Tukey's multiple comparisons test with $db/+$ excluded to determine effect of treatment. For (D-L) unpaired t-test $db/+$ vs db/db to determine effect of genotype. One-way ANOVA followed by Tukey's multiple comparisons test with $db/+$ excluded to determine effect of treatment.

Figure 5

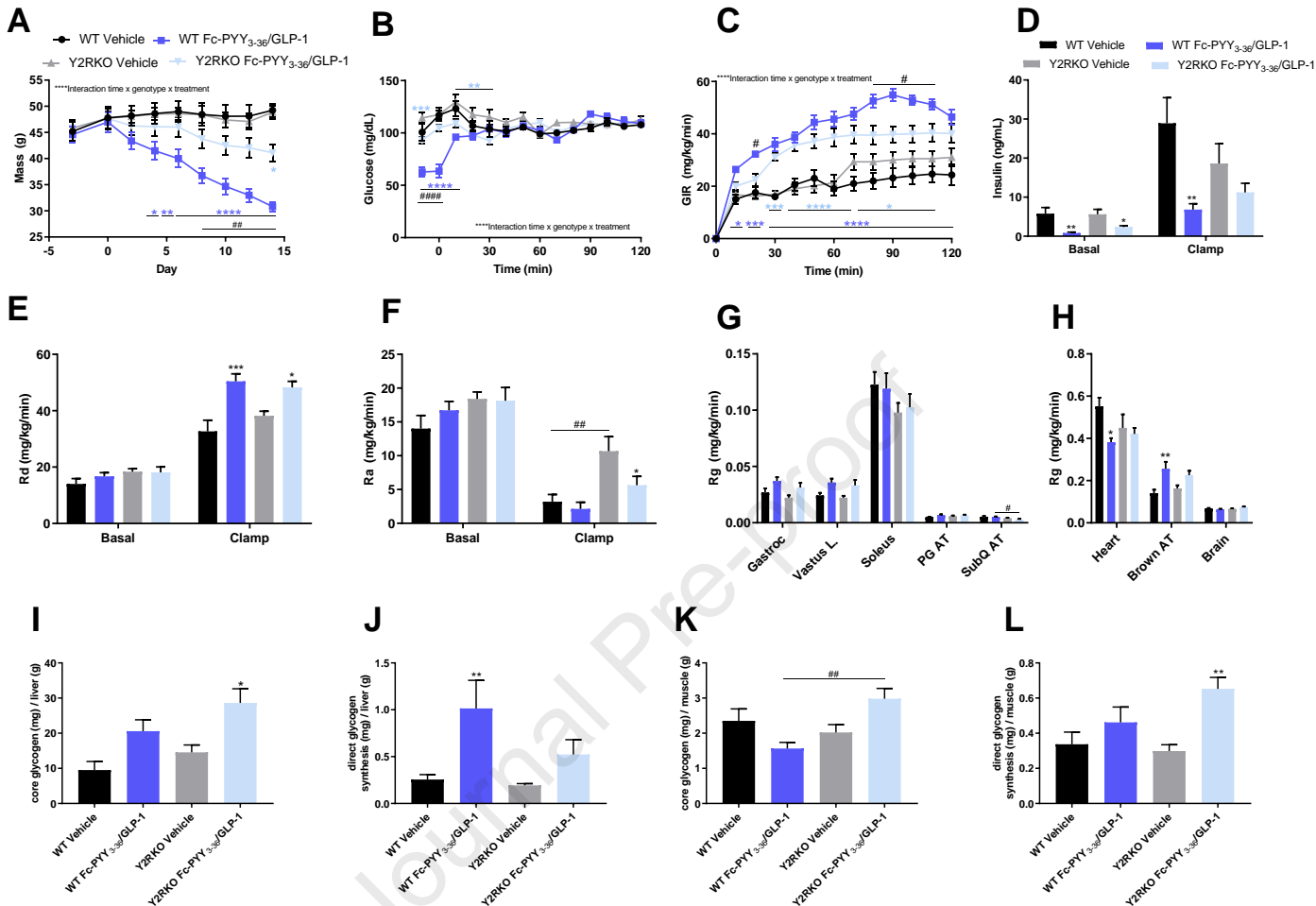


Figure 5: Hyperinsulinemic/euglycemic clamp following 2 week Fc-PYY₃₋₃₆/GLP-1 (1 mg/kg/0.15 mg/kg) treatment in DIO WT and Y2RKO mice. A) Body weight profile of study animals. B) Plasma glucose levels during the clamp. C) Glucose infusion rate required to maintain euglycemia (110 mg/dL) during the clamp. * $p \leq 0.05$ WT Vehicle vs WT Fc-PYY₃₋₃₆/GLP-1, # $p \leq 0.05$ WT Vehicle vs Y2RKO Fc-PYY₃₋₃₆/GLP-1. D) Basal and insulin-stimulated plasma insulin levels. E) Basal and insulin-stimulated peripheral glucose disposal (Rd). F) Basal and insulin-stimulated endogenous glucose production (Rg). G) Tissue-specific insulin-stimulated glucose disposal for gastrocnemius, vastus lateralis, soleus, perigonadal and subcutaneous adipose tissue and H) heart, brown adipose tissue and brain. I) Core liver glycogen. J) Direct liver glycogen synthesis. K) Core muscle glycogen. L) Direct muscle glycogen synthesis. N=5-10. * $p \leq 0.05$, ** $p \leq 0.01$, *** $p \leq 0.001$, **** $p \leq 0.0001$, vs vehicle within genotype. # $p \leq 0.05$, ## $p \leq 0.01$, ### $p \leq 0.0001$ WT vs Y2RKO within treatment. For (A-C) two-way ANOVA with repeated measures followed by Tukey's multiple comparisons test. For (D-L) two-way ANOVA followed by Sidak's multiple comparisons test.

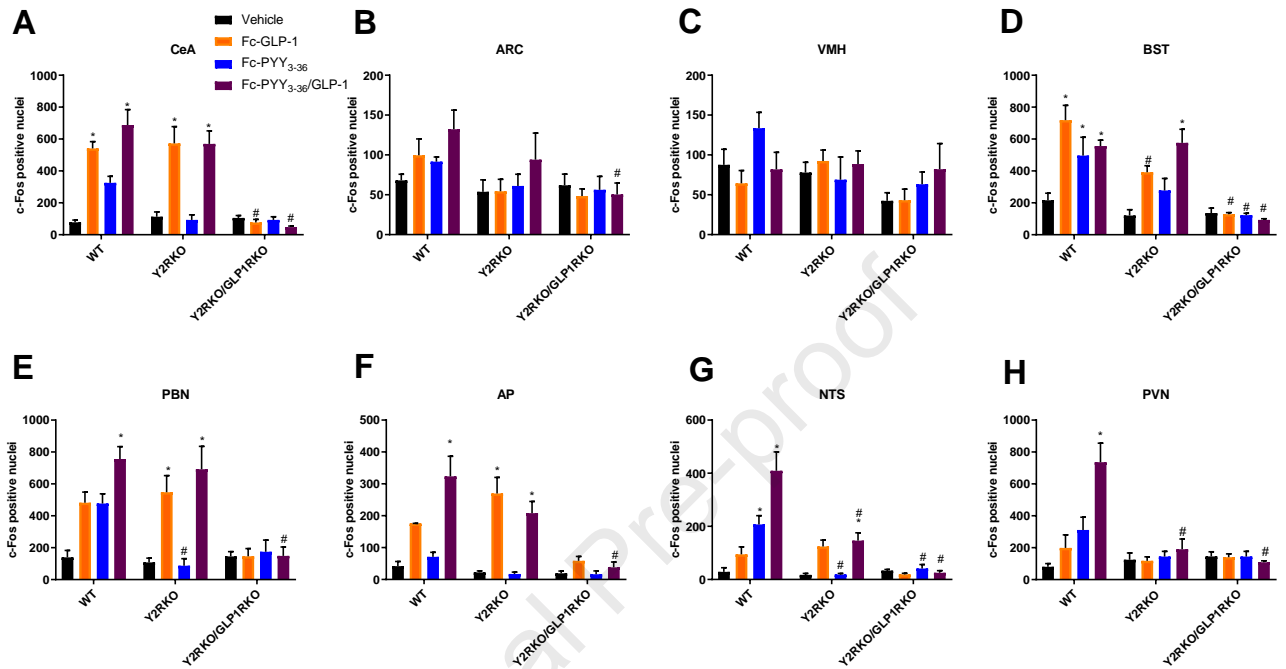


Figure 6: Quantitation of cFOS-positive cells in selected brain regions of lean WT, Y2RKO, and Y2RKO/GLP1RKO mice 4 hours following IP-administered Fc-PYY₃₋₃₆ (1.0 mg/kg), Fc-GLP-1 (0.15 mg/kg) or Fc-PYY₃₋₃₆/GLP-1 (1.0 mg/kg / 0.15 mg/kg) combination. The average stained number of cFOS positive cells in the A) central nucleus of the amygdala (CeA), B) arcuate nucleus (ARC), C) ventromedial hypothalamic nucleus (VMH), D) bed of the stria terminalis (BST), E) parabrachial nucleus (PBN), F) area postrema (AP), G) nucleus of the solitary tract (NTS), and H) paraventricular hypothalamic nucleus (PVN) are shown. * $p \leq 0.05$ vs Vehicle, same genotype # $p \leq 0.05$ vs WT, same treatment. N=2-5.

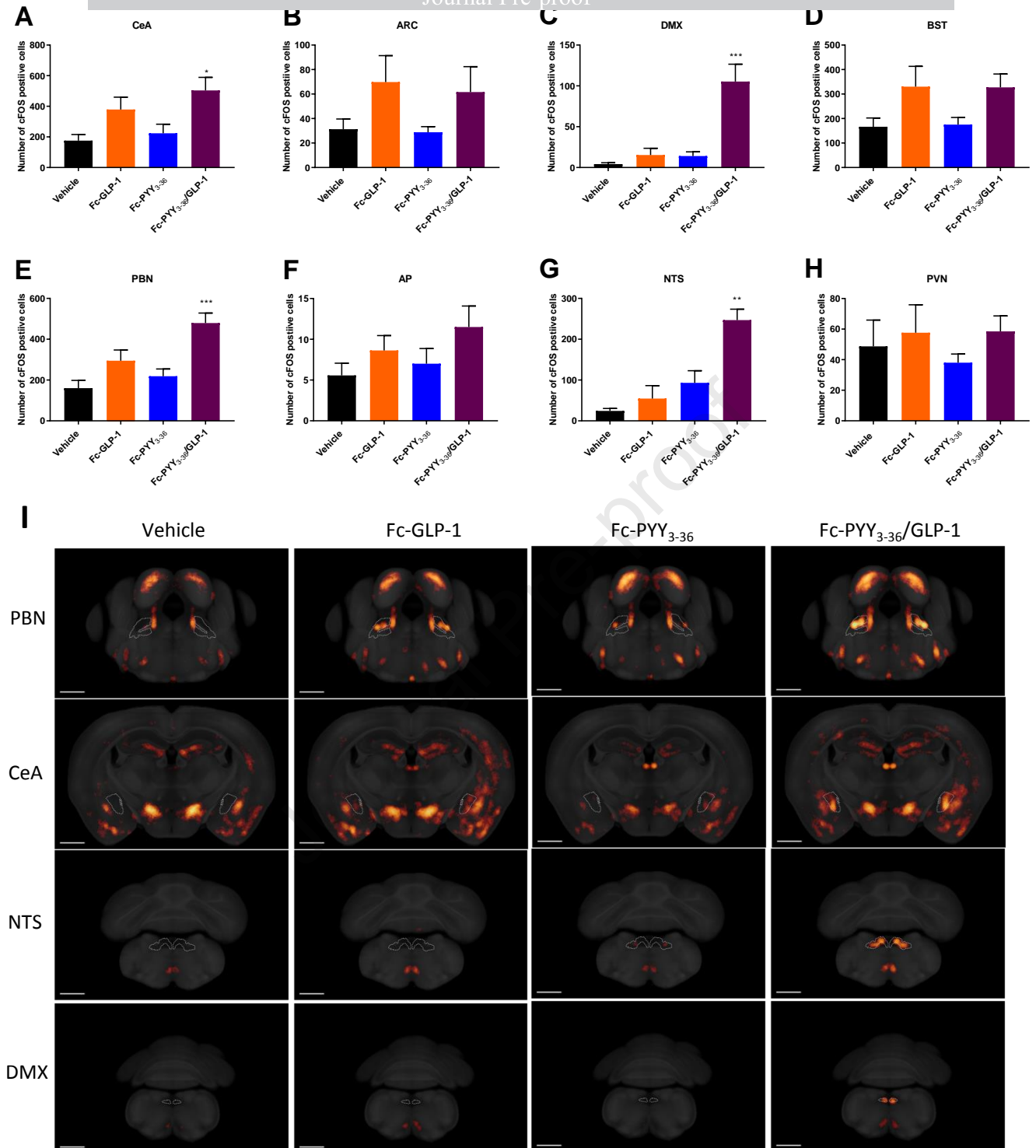


Figure 7: Whole brain cFOS quantitation of selected brain regions 24 hours following IP-administered Fc-PYY₃₋₃₆ (1.0 mg/kg), Fc-GLP-1 (0.5 mg/kg) or Fc-PYY₃₋₃₆/GLP-1 (1.0 mg/kg / 0.5 mg/kg) combination in lean C57BL6J mice. Total number of cFOS positive cells in the A) arcuate nucleus (ARC), B) paraventricular nucleus (PVN), C) area postrema (AP), D) bed of the stria terminalis (BST), E) central nucleus of the amygdala (CeA), F) parabrachial nucleus (PBN), G) nucleus of the solitary tract (NTS), H) dorsal motor nucleus of the vagal nerve (DMX) as assessed by light sheet fluorescent microscopy. I) Selected coronal sections from group averaged brains (scale bar = 1 mm). Brain regions delineated by dashed outline.

Highlights

- Long acting Peptide-YY₃₋₃₆ (Fc-PYY₃₋₃₆) and Glucagon-Like Peptide-1 (Fc-GLP-1) combination therapy induces profound weight loss and promotes diabetes remission in C57BLKS/J db/db mice.
- Fc-PYY₃₋₃₆ + Fc-GLP-1 enhances β -cell functional recovery and increases expression of key genes related to normal β -cell function.
- Improved insulin sensitivity and hepatic glycogen synthesis independent of weight loss was observed following Fc-PYY₃₋₃₆ + Fc-GLP-1 treatment.
- Fc-PYY₃₋₃₆ + Fc-GLP-1 synergistically activates discrete hypothalamic and brainstem nuclei following acute administration to potentially influence appetite control and metabolic homeostasis.